NACA

RESEARCH MEMORANDUM

EFFECT OF INLET ASPECT RATIO ON THE STARTING AND PRESSURE RECOVERY CHARACTERISTICS OF A RECTANGULAR SWEPT SCOOP INLET TESTED AT A MACH NUMBER OF 3.1

By Ernest A. Mackley

Langley Aeronautical Laboratory
Langley Field, Va.

NATIONAL ADVISORY COMMITTEE
FOR AERONAUTICS

WASHINGTON

January 13, 1958

... (is changed to Unclassified)

By authority of NASA Tech Pub Announcement #17
(OFFICER AUTHORIZED TO CHANGE)

By W Parks
NAME AND

NIC
GRADE OF OFFICER MAKING CHANGE)

16 Feb 61
DATE

NATIONAL ADVISORY COMMITTEE FOR AERONAUTICS

RESEARCH MEMORANDUM

EFFECT OF INLET ASPECT RATIO ON THE STARTING AND PRESSURE RECOVERY CHARACTERISTICS OF A RECTANGULAR SWEPT SCOOP INLET TESTED AT A MACH NUMBER OF 3.1

By Ernest A. Mackley

SUMMARY

An experimental investigation of a rectangular swept scoop inlet designed for and tested at a free-stream Mach number of 3.1 was made to determine the effect of inlet aspect ratio (height to width) on the minimum inlet starting contraction ratio (throat to frontal area) and the resulting inlet total-pressure recovery. Three simulated fuselages of varying cross-sectional width were tested at an angle of attack of 0° and an angle of yaw of 0° with and without a wedge boundary-layer diverter at a Reynolds number of approximately 2.8×10^6 based on a length of 1 inch. Inlet aspect ratio was varied between 0.5 and 4.0 in seven steps by holding the inlet height constant and varying the inlet width. Comparison of the experimental minimum starting contraction ratios with an approximate theory of inlet starting was made.

The experimental minimum starting contraction ratio decreased with increasing inlet aspect ratio and produced a trend similar to that predicted by theory with no large effects of simulated fuselage shape. For no fuselage boundary-layer diversion, good agreement with theory was obtained at inlet aspect ratios below 1.0, the starting contraction ratios becoming larger than the predicted values for aspect ratios above 1.0. The use of boundary-layer diverters on the fuselage ahead of the inlet throat increased the starting contraction ratios for low-aspect-ratio inlets, but one of the diverters gave reduced (below no diversion) starting contraction ratios above an aspect ratio of 1.35.

The maximum total-pressure recovery generally occurred just prior to inlet buzz. The maximum critical-pressure recovery obtained was 0.55 at a mass-flow ratio of 0.89 with no boundary-layer diversion, an aspect ratio of 1.5, and a contraction ratio of 0.421. The maximum overall total-pressure recovery obtained was 0.67 at a mass-flow ratio of 0.65 with the best diverter, an aspect ratio of 3.7, and a contraction ratio of 0.313.

INTRODUCTION

A rectangular scoop inlet with swept sides which was designed for high-pressure recovery and low external drag has been tested and the results are reported in reference 1. These experimental results indicated that the pressure-recovery characteristics were promising. The "starting" characteristics of this type of inlet are affected by the fuselage because it restricts the flow of air around the inlet during the starting process. The degree of this restriction is a function of the inlet aspect ratio (ratio of inlet height to width). During the starting process the air which cannot pass through the inlet throat must spill around the sides of the inlet. Consequently, for a particular aspect ratio the inlet starting characteristics are primarily a function of inlet contraction ratio (throat area to frontal area). The starting problem can be eliminated by designing for relatively large values of contraction ratio. High-pressure recoveries, however, require low values of contraction ratio. Therefore, the inlet contraction ratio should be as small as is consistent with the starting requirements. Since the starting contraction ratio may be only approximated by theoretical means, an experimental investigation is required to determine actual values.

The purpose of this investigation was to determine the effect of inlet aspect ratio on the minimum starting contraction ratio, total-pressure recovery, and mass-flow characteristics of the inlet and to compare the results with an approximate theory for starting at the design Mach number. Rectangular inlets of aspect ratios 0.5, 0.75, 1.0, 1.5, 2.0, 3.0, and 4.0 were designed for and tested at a free-stream Mach number of 3.1, and a Reynolds number of about 2.8×10^6 (based on a length of 1 inch), at an angle of attack of 0° with simulated fuselage sections of three cross-sectional widths ahead of the inlet. The inlet contraction ratio was varied as required for starting and tests were made with and without fuselage boundary-layer diversion immediately ahead of the inlet throat.

SYMBOLS

A	area, sq in.
$\left[\frac{A^*}{A}\right]_\infty$	isentropic area ratio for the free-stream Mach number
AR	inlet aspect ratio A_1/w^2 or h_1/w for a rectangular frontal area

h	inlet or stream tube height normal to average streamline, in.
M	Mach number
$\frac{m_4}{m_\infty}$	ratio of mass flow through duct to mass flow through a free-stream tube of cross-sectional area A_1 equal to projected inlet frontal area
p	pressure, lb/sq in. abs
$\frac{p_{t,4}}{p_{t,\infty}}$	total-pressure recovery or ratio of area weighted average total pressure to free-stream total pressure
R	distance from inboard inlet lip to assumed normal shock wave, in.
S	sonic flow area, sq in.
w	inlet width, in.
β	angle of first shock wave from compression surface and angle of leading edge of inlet side wall relative to free stream, deg
Δ	total flow deviation or turning of compression surface, deg
θ	two-dimensional shock-wave angle giving sonic velocity and a flow deflection ϕ behind wave, deg
ϕ	flow deflection for shock wave of angle θ, deg

Subscripts:

∞	free-stream conditions
1	station of outboard inlet lip
2	condition between 1 and 3 and behind assumed normal shock wave moving into inlet
3	inlet minimum section or throat
4	diffuser exit or compressor face station
a	available

b,c referring to portions of theoretical capture area flowing past station 1

d referring to portions of free stream passing through conical shaped wave at sides of inlet

r required

s at sides of inlet

t stagnation conditions

APPROXIMATE THEORETICAL DETERMINATION OF INLET STARTING AT INLET DESIGN MACH NUMBER

Starting at the design Mach number of a supersonic swept scoop inlet of the type shown in the photographs of figure 1 and the sketch in figure 2 is a function of the geometric contraction ratio A_3/A_1, the supersonic total-pressure recovery, and the amount of flow that can be spilled around the inlet. The spillage is mainly a function of the inlet geometry and free-stream Mach number. An approximate theory for determining the minimum starting contraction ratio has been presented in references 2 and 3. In this paper the theory has been revised to provide for some difference in initial assumptions.

Assumptions made and used for the analysis of starting were: the spillage flow outside the inlet side walls was two dimensional, that is, it had no velocity component toward or away from the fuselage; the assumed wave EDD' (fig. 3) was conical in shape and could always be adequately represented (between stations 1 and 3) by a circular arc in a plane parallel to the free stream and normal to the inlet side walls (fig. 3(b)); the portion of the moving wave immediately ahead of and between the inlet side walls was normal to the free stream; and all boundary-layer effects were neglected.

In the starting process a normal shock wave was assumed to move downstream into the inlet. With the normal shock wave at a particular station, as in figure 3, the portion, h_b by w, of the theoretical free-stream capture area A_1 was assumed to pass through the oblique shock wave, part of the isentropic compression, the normal shock, and through the inlet minimum section. If boundary-layer effects are neglected, the remaining minimum area for a particular inlet contraction ratio determined the portion of h_c by w that must be spilled around the inlet.

From the considerations given in the appendix, the starting contraction ratio for a particular swept scoop inlet may be determined by the equation

$$\frac{A_3}{A_1} \geq \frac{1}{wAR}\left(\frac{A^*}{A}\right)_\infty \left[\frac{h_b}{\left(\frac{p_{t,2}}{p_{t,\infty}}\right)_b} + \frac{h_c}{\left(\frac{p_{t,2}}{p_{t,\infty}}\right)_c}\right] -$$

$$\left(\frac{R}{R_1}\right)^2\left(\frac{R_1^2}{A_1}\right)\tan\beta\left[\cos(\theta - \phi) - \frac{\left(\frac{A^*}{A}\right)_\infty \cos\theta}{\left(\frac{p_{t,2}}{p_{t,\infty}}\right)_d}\right]$$

In order to use this relation, the variation of theoretical total-pressure recovery with flow deviation and shock-wave position must be known. The total-pressure recovery through the curved shock wave outside the inlet side walls was assumed to be a constant and the value used was that for a two-dimensional shock wave at the free-stream Mach number of 3.1 and a shock angle of 76° 59' (that is, average of 90° and the value at the sonic point $\theta = 63° 58'$).

Typical results obtained from this equation for a Mach number of 3.1 are shown in figure 4. It can be seen that, for a particular aspect ratio, the contraction ratio increases to a maximum and then decreases as the normal shock moves toward the inlet throat $\left(\frac{R}{R_1}\right.$ decreasing$\left.\right)$. The maximum values of contraction ratio (largest values of A_3 with respect to A_1) for each aspect ratio gives the variation of starting contraction ratio shown in figure 5. Also shown in figure 5 for comparison are a theoretical curve and experimental data taken from reference 2 and a theoretical curve calculated by using the method outlined in the appendix and the spillage area S_s at the sides of the inlet as given in reference 3.

As the moving wave approaches the inboard lip (R and h_c approach zero and h_b approaches h_1), the accuracy of the approximation decreases because of the small values involved and the increased chance of error in

the initial assumptions of constant wave shape, and so forth. However, when the inlet is started, the allowable contraction ratio at a particular Mach number ceases to be a function of inlet width and is simply a function of the total-pressure recovery or from equation (A9):

$$\lim_{R \to 0} \left(\frac{A_3}{A_1}\right) = \left(\frac{A^*}{A}\right)_\infty \frac{1}{\left(\frac{p_{t,3}}{p_{t,\infty}}\right)}$$

APPARATUS AND TESTS

This investigation was conducted in a 9- by 12-inch blowdown jet of the Langley Gas Dynamics Branch at a Mach number of 3.1 and angles of attack and yaw of 0°. The test setup (fig. 6) was generally similar to that of reference 1, the Reynolds number (based on a length of 1 inch) for the tests being approximately 2.8×10^6.

Models

Seven models of a supersonic swept scoop inlet (figs. 1 and 2) were tested during this investigation. The general aerodynamic design of the inlets was similar to that of reference 1. A 12° initial flow deflection was followed by a curved surface approximating isentropic turning (calculated in increments of two degrees of turning) as shown in figure 7. The inlet side walls were swept back along the first shock wave at 28° 32' (β) to the free-stream direction. The total amount of flow turning was varied by altering the compression surface as required to change the inlet contraction ratio $\frac{A_3}{A_1}$. The variation of the total flow deviation and the resulting theoretical total-pressure recovery (including normal-shock losses) as a function of contraction ratio is shown in figure 8.

With the inlet height constant at 2 inches, models were constructed of different widths to give aspect ratios of 0.5, 0.75, 1.0, 1.5, 2.0, 3.0, and 4.0. Three simulated fuselage cross sections were used in front of the inlet. (See fig. 2.) Fuselage I was a flat, tunnel-spanning section; fuselage II was 2 inches wider than the inlet - that is, a 1-inch-radius section on each side of the inlet; and fuselage III was rectangular and the same width as the inlet. The models were of steel

and plastic construction, plastic being used for the internal surfaces that were subject to alteration.

The subsonic diffuser exit height was fixed $(h_4 = 3.0)$ with the flow at this station parallel to the free-stream direction but was offset inboard as shown in figure 2. The contour of the diffuser was arbitrarily faired between the inlet minimum section and the diffuser exit, a compromise being made between gradual diffusion before turning and having as long a radius turn as possible. For the inlets tested, the duct height normal to the mean streamline increased as shown in figure 9.

Tests were made first without removal of the fuselage boundary layer in front of the inboard inlet lip. In an effort to improve the starting characteristics, a flat wedge-like boundary-layer diverter was installed ahead of the inboard lip. The details of the diverters are shown in figure 10. Diverter 1 was made with flat surfaces on the sides at an angle to the fuselage of 40° at the apex in a plane normal to the free stream. This angle increased downstream of the apex to near 90° immediately ahead of the inlet-fuselage juncture. Diverter 2, a modification of diverter 1, was thinned near the apex (fig. 10(a)) and the sides were faired to the fuselage downstream of the corresponding point of diverter 1. Diverter 2 approximated a flat plate near the tip with a faired support to the fuselage. Since it was considered desirable to maintain a low included angle on the wedge, the wedge diverters for the low aspect ratios (wide inlets) became too long to be effective; therefore, a "bump" or compression-type diverter was tested. (See fig. 10(b).) This diverter with the increased pressure on the wedge surface caused the boundary layer to flow toward the lower pressure at the sides of the inlet.

Tests, Procedure, and Measurements

The contraction of each inlet was altered by changing the total-flow deviation of the inlet. Experimental contraction ratios were computed from measurements of the actual minimum height h_3. Inlet total-pressure recovery and mass flow were measured; also shadow photographs and visual schlieren observations were made for each test. Inlet starting observed by use of the schlieren system was verified by the mass-flow data and inspection of the shadow photographs.

Pressure measurements at the diffuser exit were made with a nine-tube total-pressure rake located on the vertical center line of the duct and eight wall static orifices (fig. 11) located around the periphery of the duct. An area-weighted average total-pressure recovery is used in the present paper. This usage is considered to be valid since the Mach numbers at the rake station were below 0.2 for the higher pressure

recoveries. The mass flow entering the inlet was measured by an orifice plate located as shown in figure 6. Two orifice sizes were used interchangeably in the same pipe to handle the range of mass flow encountered in the tests; the orifice installation met the specifications set forth in reference 4.

The mass-flow ratios for all inlets are based on the projected frontal area of the inlet minus the projected frontal area of the diverter, if any. For the bump diverter which created a compression wave, mass-flow ratios over 1.0 are possible. The mass-flow ratios and measured total-pressure recovery are considered to be accurate within ±2 percent.

RESULTS AND DISCUSSION

Determination of Starting Contraction Ratio

The typical shadow photographs of figure 12 show the effect on the inlet flow pattern of varying inlet contraction ratio. The unstarted inlet (fig. 12(a)) with no boundary-layer diversion had a strong oblique wave and accompanying separation in the "crotch" of the inlet (between the fuselage and inlet side wall). As the minimum area A_3 was increased, this separated area moved toward the inlet throat and decreased in size. Figure 12(c) shows a configuration that was considered started but was a borderline case. The shock wave originating at the point of boundary-layer separation on the fuselage curved or wrapped around the inlet as the flow expanded to free-stream conditions. This curved wave caused refraction of light and made the separated portion of the flow appear larger than it actually was. This is evident when a shadow photograph with flow past the model is compared with a corresponding photograph with no flow. Regions of refracted light can also be seen as white lines along the inlet side walls. A typical case of a completely started inlet configuration is shown in figure 12(d). The flow depicted here occurred most often with fuselage boundary-layer diversion but was possible in many cases without boundary-layer diversion.

Maximum mass-flow ratios of at least 0.98 were generally considered to be necessary to establish a started condition. In some cases starting was considered to be possible for mass-flow ratios as low as 0.96, depending upon the appearance in the shadow photographs of the flow in the crotch.

From the appearance of the flow in the shadow photographs it would appear that the flow model assumed in the original starting was oversimplified. The existence of a stationary normal-shock wave in the crotch

of the inlet was precluded by separation of the fuselage boundary layer (ref. 5) because of the excessive pressure rise of a normal wave. The shadow photographs show an oblique wave existed at nearly a constant angle (or pressure rise) regardless of the position of the point of separation relative to the inlet throat. This position must still be determined by the spillage requirements back of the oblique wave - that is, the wave shape at the sides of the inlet, the inlet aspect ratio, and the contraction ratio. Some of the separated flow undoubtedly entered the inlet and decreased the effective inlet throat area (especially at low back pressures). The spillage area at the sides of the inlet was less than that calculated from the assumptions made, but the losses through the oblique wave were much less than the assumed normal shock losses (approximately 7 percent of $p_{t,\infty}$ instead of 70 percent). These factors tend to compensate each other, but the spillage of the separated flow around the inlet is unpredictable.

Effect of Inlet Aspect Ratio on the Inlet Starting Characteristics

Without boundary-layer diversion.- The effect of inlet aspect ratio on the starting contraction ratio for the three simulated fuselage sections tested with no boundary-layer diversion is shown in figure 13. The experimental starting contraction ratio $\frac{A_3}{A_1}$ generally decreased with increasing inlet aspect ratio, and the effects of the simulated fuselage cross-sectional shapes were small. The maximum mass-flow ratios are given for each point. Also the faired experimental curve is shown as a dashed line for the high-aspect-ratio inlets wherever the results did not show the actual starting as established by the criterion given previously.

The theoretical variation in starting contraction ratio with inlet aspect ratio is shown in figure 13 for comparison purposes. It can be seen that for no boundary-layer diversion the experimental starting contraction ratios are generally consistent with the theoretical values at low aspect ratios but the started configurations at aspect ratios above 1.0 had contraction ratios up to 18 percent higher than predicted. This greater disagreement with increasing aspect ratios may be partially due to an internal boundary-layer effect since, as the width of the inlet was decreased, the amount of boundary layer on the internal supersonic surfaces became a larger percentage of the flow through the inlet throat and greater internal boundary-layer effects could be expected. However, if the three-dimensional oblique wave that originated at the point of separation and wrapped around the inlet remained nearly geometrically

similar regardless of position relative to the inlet throat, the amount of separated flow entering the inlet for a high aspect ratio should be somewhat less than that for a low aspect ratio at the same mass-flow ratio $\frac{m_4}{m_\infty}$. This depends, of course, on the spillage of the separated flow which is considered relatively unpredictable.

With boundary-layer diversion.- A flat-wedge boundary-layer diverter (diverter 1, fig. 10(a)) was placed on the fuselage immediately ahead of the beginning of the inlet throat. The presence of the diverter decreased the effective inlet height and, as a result, the inlet aspect ratio. The variation of starting contraction ratio with inlet aspect ratio using boundary-layer diversion (diverter 1) is shown in figure 14 for the three simulated fuselage sections tested. The effect of fuselage cross section was again small with the started configurations again showing decreasing contraction ratio $\frac{A_3}{A_1}$ with increasing inlet aspect ratio. The use of diverter 1 gave the adverse effect of generally increasing the starting contraction ratio over no boundary-layer diversion, especially for the low-aspect-ratio inlets. However, the trend of changing contraction ratio with aspect ratio is more nearly consistent with the theoretical variation, although the values of $\frac{A_3}{A_1}$ were approximately 18 percent higher than the theoretical values.

Since the diverter wedges were kept at a relatively low angle in the plan form (fig. 10), the length increased with decreasing inlet aspect ratio; thus their purpose was defeated. The widest inlet (aspect ratio 0.44) was impossible to start by using a flat-wedge diverter. A "bump" type diverter (fig. 10(b)) was used for some tests with fuselages II and III and allowed the inlet to start as shown in figure 14. The mass-flow ratio for the tests with the bump diverter was based on the total frontal area of the inlet minus the projected frontal area of the diverter in the same manner as was done for the flat-wedge diverters. With the compression on the bump it was possible to obtain mass flows over 1.0 as shown for the started configurations (aspect ratio 0.44, fig. 14, and table I(f)).

The variation in starting contraction ratio with inlet aspect ratio using boundary-layer diverter 2 (fig. 10(a)) is shown in figure 15. The effect of fuselage shape was small as it was for no diverter and diverter 1. The trend of decreasing starting contraction ratio with increasing aspect ratio was still present. The use of diverter 2, a modification of diverter 1, resulted in generally better agreement between the experimental and theoretical starting contraction ratios

than for diverter 1. Diverter 2 also gave better agreement with theoretical starting contraction ratios than no diverter for aspect ratios above 1.35. The reason for the adverse effect of the boundary-layer diverters on the starting contraction ratios for the low-aspect-ratio inlets is not clear from the results of this investigation.

Total-Pressure Recovery and Mass-Flow Variations

Typical variations of total-pressure recovery with mass-flow ratio for various inlet aspect ratios and contraction ratios with no boundary-layer diversion are shown in figures 16, 17, and 18 for fuselages I, II, and III, respectively. Similar variations with boundary-layer diversion, diverter 1, are shown in figures 19, 20, and 21, and for diverter 2 in figures 22, 23, and 24. In these figures the faired curves are shown as dotted lines where there was evidence of a discontinuous change in mass-flow ratio with total-pressure recovery. For the data given in figures 16 to 24, the lowest mass-flow ratio point on each curve was taken just prior to inlet buzz; no data were taken during buzz. Generally buzz or inlet instability for this type of inlet occurs suddenly and rather violently when the minimum mass flow is reached. This was especially true for the present configurations for which there was only a small amount of subcritical stability. In the cases where separation on the fuselage existed at high back pressure, small fluctuations were noted in the flow near the inlet crotch immediately prior to inlet buzz.

It may be noted from figures 16 to 24 for the high aspect ratios that maximum $\frac{p_{t,4}}{p_{t,\infty}}$ occurred at low mass-flow ratios. For these cases as well as the unstarted inlets at all back pressures, separation was present on the fuselage ahead of the inlet throat. The oblique wave standing on the diverter, or fuselage, was at a nearly constant angle and the losses for the flow through this wave and outside the separated region were small. At high back pressures and low mass-flow ratios a large part of the separated flow was evidently spilled around the inlet since the total-pressure recoveries were relatively high compared with the theoretical recoveries for a particular amount of flow turning. Also the subsonic losses might be expected to decrease as the mass flow and internal Mach numbers decrease.

A discontinuous change in mass flow with total-pressure recovery was found in some cases as is shown in figures 16(c), 17(c), and 22(b). This change was a result of the sudden occurrence of boundary-layer separation in the crotch and the concomitant spillage. Varying spillage rates are noticeable in the changing slopes of the low-pressure-recovery portions of the curves of mass flow against total-pressure recovery.

(See figs. 16 to 22.) These slopes generally became less as the aspect ratio increased. This loss of mass flow was considered to be the internal boundary layer spilling around the inlet side walls and became greater as the internal boundary layer became a larger part of the entering flow (aspect ratio increasing). The slopes in the low-pressure-recovery region for fuselages I and II were greater than those for fuselage III; thus some variation in spillage around the inlet because of fuselage cross-sectional shape was indicated. The use of a diverter gave a similar effect (increased slope) for a particular aspect ratio, diverter 2 being slightly more effective in this respect.

Effects of Inlet Aspect Ratio on the Maximum Total-Pressure Recovery

Summary curves of the maximum total-pressure recoveries taken from figures 16 to 24 and more similar data are plotted as a function of inlet aspect ratio in figures 25, 26, and 27. Maximum $\frac{p_{t,4}}{p_{t,\infty}}$ points generally occurred just prior to inlet buzz or flow instability. These figures show a trend of increasing maximum total-pressure recovery with increasing inlet aspect ratio which is a reflection of the general trend of decreasing starting contraction ratio $\frac{A_3}{A_1}$ with increasing inlet aspect ratio. The maximum critical total-pressure recovery obtained during these tests was 0.55 for an aspect ratio of 1.5, $\frac{A_3}{A_1} = 0.421$, $\frac{m_4}{m_\infty} = 0.89$, and fuselage I with no diversion. The maximum overall value of pressure recovery was 0.67 at a low mass-flow ratio $\left(\frac{m_4}{m_\infty} = 0.65\right)$ for an aspect ratio of 3.7, $\frac{A_3}{A_1} = 0.313$, fuselage III, and diverter 2.

The theoretical total-pressure recovery (including normal shock losses), shown in figures 25, 26, and 27, represents the maximum obtainable for the experimental starting $\frac{A_3}{A_1}$ curves in figures 13, 14, and 15 and was obtained by using figure 8. The theoretical pressure-recovery curves are shown as dashed lines where necessary to correspond to figures 13, 14, and 15. The experimental total-pressure-recovery data

showed similar trends as the theoretical curves but were 10 to 20 percent lower. No specific effort was made to increase the experimental total-pressure recovery by modifications to the inlet other than the fuselage boundary-layer diverters shown.

The configurations which were started at low pressure recovery or in the supercritical region are noted on the figures. It can be seen that in some cases the maximum total-pressure recovery of the inlets which were started at low pressure recovery was slightly lower than the unstarted inlets of the same aspect ratio. As stated previously in the section entitled "Total-Pressure Recovery and Mass-Flow Variations" in the present tests with the inlets operating at high back pressures and low mass-flow ratios, the total-pressure losses from free stream to the diffuser exit were not high although this would be a relatively high drag condition because of the spillage. The values of mass-flow ratio and contraction ratio for the experimental points in figures 25, 26, and 27 are tabulated (table I) in order of decreasing total-pressure recovery to give a correlation of the data with that of the preceding figures.

The variations of minimum starting contraction ratios caused by the use of boundary-layer diverters were reflected in the maximum total-pressure recoveries. The use of diverter 1 generally gave decreases of about 0.02 to 0.06 in maximum recovery compared with no boundary-layer diversion. Similar decreases were found for diverter 2 with fuselages I and II, whereas small increases were found for diverter 2 with fuselage III.

The differences in maximum total-pressure recovery between fuselages I and II configurations were generally small (up to 0.03), whereas fuselage III configurations gave general increases in total-pressure recovery over fuselage I (up to 0.11).

SUMMARY OF RESULTS

An experimental investigation has been made at a free-stream Mach number of 3.1 to determine the effect of inlet aspect ratio (height to width) on the minimum inlet starting contraction ratio and the resulting total-pressure recovery. The experimental results have been compared with the results from an approximate theory of starting. The aspect ratios for the seven inlet configurations varied from 0.5 to 4.0. Three simulated fuselages of varying cross-sectional width, with and without fuselage boundary-layer diversion immediately ahead of the inlet throat, were tested at a Reynolds number of approximately 2.8×10^6 based on a length of 1 inch. The following results were obtained:

1. The minimum starting contraction ratio decreased with increasing inlet aspect ratio, the effects of simulated fuselage cross-sectional shape being small. The use of boundary-layer diverters increased the minimum starting contraction ratios for low aspect ratios, but one of these diverters reduced the starting contraction ratios for aspect ratios above 1.35.

2. The experimental values of minimum starting contraction ratio agreed well with theoretical values for low-aspect-ratio inlets with no boundary-layer diversion. At aspect ratios above 1.35, the starting contraction ratios, either with or without a diverter, were increasingly higher than the predicted values.

3. The maximum pressure recovery, which generally occurred just prior to inlet buzz, increased with increasing inlet aspect ratio and decreasing contraction ratio. The effects on the total-pressure recovery of the simulated fuselage cross-sectional shape were small for the two wider fuselage configurations. The narrow fuselage (same width as the inlet) gave increases in total-pressure recovery up to 0.11 over the widest fuselage configuration. Maximum critical total pressure found was 0.55 at a mass-flow ratio of 0.89 for no boundary diversion, an aspect ratio of 1.5, and a contraction ratio of 0.421. Maximum overall pressure recovery was 0.67 at a mass-flow ratio of 0.65 with the best of two diverters tested, an aspect ratio of 3.7, and a contraction ratio of 0.313.

Langley Aeronautical Laboratory,
National Advisory Committee for Aeronautics,
Langley Field, Va., September 26, 1957.

APPENDIX

DETERMINATION OF INLET STARTING

The starting of a swept scoop inlet of the type shown in figure 1 at the design Mach number is a function of the geometric contraction ratio $\frac{A_3}{A_1}$, the supersonic total-pressure recovery, and the amount of flow that can be spilled around the inlet. The spillage is mainly a function of the inlet geometry, the physical system of spillage, and the free-stream Mach number.

The spillage flow was assumed to be two dimensional and to occur behind a shock wave which was normal in front of the inlet and wrapped around the inlet at the sides. The wave at the sides EDD' (fig. 3) was assumed to be conical in shape (apex at the edge of the swept inlet side wall and base in the plane of the fuselage) and to be always adequately represented between stations 1 and 3 by a circular arc in a plane parallel to the free stream and normal to the inlet side walls.

In the starting process the normal-shock wave was assumed to move into the inlet in stationwise steps. With the wave at a particular position (as in fig. 3) the portion $h_b \times w$ of the theoretical capture area A_1 was assumed to pass through the oblique wave, part of the isentropic compression, the normal wave, and through a sonic inlet throat. If boundary-layer effects are neglected, the remaining throat area for a particular inlet contraction ratio determined what portion of $h_c \times w$ must be spilled around the inlet. These considerations give the basic equation:

$$S_a \geq S_r$$

or

$$A_3 + S_{a,s} \geq S_r \tag{A1}$$

For the wave geometry assumed, it is possible to determine the sonic area required:

$$S_r = S_{r,A_1} + S_{r,d} \tag{A2}$$

where S_{r,A_1} is the sonic flow area required by the free-stream tube of area A_1 and $S_{r,d}$ is the sonic flow area required by the free-stream tube passing through the conical waves at the sides of the inlet for an average total-pressure recovery $\left(\frac{p_{t,2}}{p_{t,\infty}}\right)_d$. The term S_{r,A_1} becomes a function of the position of the moving wave since the average pressure recovery of the outboard portion of the entering inlet flow h_b (fig. 3(a)) changes with shock wave position. Then

$$S_{r,A_1} = \frac{A_1}{h_1}\left(\frac{A^*}{A}\right)_\infty \left[\frac{h_b}{\left(\frac{p_{t,2}}{p_{t,\infty}}\right)_b} + \frac{h_c}{\left(\frac{p_{t,2}}{p_{t,\infty}}\right)_c}\right]$$

or

$$S_{r,A_1} = \frac{h_1}{AR}\left(\frac{A^*}{A}\right)_\infty \left[\frac{h_b}{\left(\frac{p_{t,2}}{p_{t,\infty}}\right)_b} + \frac{h_c}{\left(\frac{p_{t,2}}{p_{t,\infty}}\right)_c}\right] \tag{A3}$$

It was previously assumed that the moving wave outside the inlet side walls could always be described by a circular arc in a plane parallel to the free stream and normal to the inlet side walls. The radius of this arc is the distance from the swept inlet side wall to the normal wave. In the plane of the fuselage this radius is the position R of the normal wave relative to the inboard inlet lip. This results in conical shaped wave which decreases in size but remains geometrically similar as R decreases. The sonic flow area required for the curved waves at both sides of the inlet is then

$$S_{r,d} = \left(\frac{A^*}{A}\right)_\infty \frac{R^2 \tan \beta \cos \theta}{\left(\frac{p_{t,2}}{p_{t,\infty}}\right)_d} \tag{A4}$$

Then from equations (A2), (A3), and (A4),

$$S_r = \frac{h_1}{AR}\left(\frac{A^*}{A}\right)_\infty \left[\frac{h_b}{\left(\frac{p_{t,2}}{p_{t,\infty}}\right)_b} + \frac{h_c}{\left(\frac{p_{t,2}}{p_{t,\infty}}\right)_c}\right] + \left(\frac{A^*}{A}\right)\frac{R^2 \tan \beta \cos \theta}{\left(\frac{p_{t,2}}{p_{t,\infty}}\right)_d} \tag{A5}$$

Next, the total sonic spillage area available at the sides of the inlet is determined. Isentropic flow is assumed between the wave EDD' (fig. 3(a)) and the sonic plane EHD'. The side ED' of the sonic plane EHD' is a generatrix of the conical wave EDD'. From the geometry shown in figure 3(a) the area of sonic plane for one side of the inlet is then:

$$\text{Area (EHD')} = \frac{R^2}{2}\left[\tan^2\beta + \cos^2\theta\right]^{1/2} \tag{A6}$$

The derivation of this equation is given in reference 3. The area of the plane EHD' is used as the sonic spillage area on one side of the inlet in reference 3. However, although the plane does contain the sonic points on the spillage streamlines for the assumptions made, the flow velocity is not necessarily normal to the plane. For the present paper the flow velocity at D'H was considered to be at some constant angle to the free stream ϕ in a plane parallel to the fuselage. The angle ϕ used was the flow deflection giving a Mach number of one behind a two-dimensional free-stream shock wave. The sonic spillage area available on one side of the inlet was considered to be the projection of the sonic plane on a plane normal to the exiting streamlines, which were previously assumed to be parallel to the plane of the fuselage. This projection is the plane E"HD" (see fig. 3(a)). The total sonic spillage area available is twice the area of E"HD" or $S_{a,s}$

$$S_{a,s} = R^2 \tan \beta \cos(\theta - \phi) \tag{A7}$$

Substituting equations (A5) and (A7) into equation (A1) gives

$$A_3 + R^2 \tan \beta \cos(\theta - \phi) \geq \frac{h_1}{AR}\left(\frac{A^*}{A}\right)_\infty \left[\frac{h_b}{\left(\frac{p_{t,2}}{p_{t,\infty}}\right)_b} + \frac{h_c}{\left(\frac{p_{t,2}}{p_{t,\infty}}\right)_c}\right] + \left(\frac{A^*}{A}\right)_\infty \frac{R^2 \tan \beta \cos \theta}{\left(\frac{p_{t,2}}{p_{t,\infty}}\right)_d}$$

or

$$A_3 \geq \frac{h_1}{AR}\left(\frac{A^*}{A}\right)_\infty \left[\frac{h_b}{\left(\frac{p_{t,2}}{p_{t,\infty}}\right)_b} + \frac{h_c}{\left(\frac{p_{t,2}}{p_{t,\infty}}\right)_c}\right] - R^2 \tan \beta \left[\cos(\theta - \phi) - \left(\frac{A^*}{A}\right)_\infty \frac{\cos \theta}{\left(\frac{p_{t,2}}{p_{t,\infty}}\right)_d}\right] \tag{A8}$$

Equation (A8) in terms of contraction ratio and normal-wave-position parameter is then

$$\frac{A_3}{A_1} \geq \frac{1}{wAR}\left(\frac{A^*}{A}\right)_\infty \left[\frac{h_b}{\left(\frac{p_{t,2}}{p_{t,\infty}}\right)_b} + \frac{h_c}{\left(\frac{p_{t,2}}{p_{t,\infty}}\right)_c}\right] - \left(\frac{R}{R_1}\right)^2 \left(\frac{R_1^2}{A_1}\right) \tan \beta \left[\cos(\theta - \phi) - \left(\frac{A^*}{A}\right)_\infty \frac{\cos \theta}{\left(\frac{p_{t,2}}{p_{t,\infty}}\right)_d}\right] \tag{A9}$$

From this equation the contraction ratio necessary to allow the inlet to start may be calculated for a particular normal wave position $\frac{R}{R_1}$.

REFERENCES

1. Comenzo, Raymond J., and Mackley, Ernest A.: Preliminary Investigation of a Rectangular Supersonic Scoop Inlet With Swept Sides Designed for Low Drag at a Mach Number of 2.7. NACA RM L52J02, 1952.

2. Ferri, Antonio: Recent Developments in the Design of Supersonic Scoop Diffusers. Wright Aero. Rep. No. 1692, Supersonic Inlet Symposium, Curtiss-Wright Corp. (Wood-Ridge, N. J.), Jan. 23, 1953.

3. Himka, Theodore: Methods of Starting Scoop-Type Inlets. Wright Aero. Rep. No. 1692, Supersonic Inlet Symposium, Curtiss-Wright Corp. (Wood-Ridge, N. J.), Jan. 23, 1953.

4. Anon.: Measurement of Quantity of Materials. Supplement on Instruments and Apparatus, pt. 5, ch. 4, Power Test Codes, A.S.M.E., 1949, pp. 5-64.

5. Chapman, Dean R., Kuehn, Donald M., and Larson, Howard K.: Preliminary Report on a Study of Separated Flows in Supersonic and Subsonic Streams. NACA RM A55L14, 1956.

TABLE I

TOTAL-PRESSURE RECOVERIES WITH CORRESPONDING MASS FLOW AND CONTRACTION RATIO

(a) Fuselage I, no diverter, figure 25(a)

AR	$\left(\frac{p_{t,4}}{p_{t,\infty}}\right)_{max}$	$\frac{m_4}{m_\infty}$	$\frac{A_3}{A_1}$
0.75	0.44	[a]0.95	0.433
1.0	.52	[b].95	.395
1.5	.55	[a].89	.421
2.0	.54	[a].84	.394
2.0	.51	.64	.331
3.0	.58	.58	.338
3.0	.56	.74	.343
3.0	.42	.56	.259
4.0	.61	.35	.290
4.0	.58	.58	.343
4.0	.55	.41	.278

(b) Fuselage II, no diverter, figure 25(b)

AR	$\left(\frac{p_{t,4}}{p_{t,\infty}}\right)_{max}$	$\frac{m_4}{m_\infty}$	$\frac{A_3}{A_1}$
0.5	0.41	0.90	0.435
.75	.45	[a].87	.446
1.0	.54	[a].96	.395
1.5	.55	[a].89	.422
2.0	.55	[a].88	.394
2.0	.54	----	.314
2.0	.52	.82	.343
3.0	.59	.64	.343
3.0	.59	[a].62	.350
3.0	.55	.63	.314
4.0	.63	.55	.290
4.0	.61	.58	.314

(c) Fuselage III, no diverter, figure 25(c)

AR	$\left(\frac{p_{t,4}}{p_{t,\infty}}\right)_{max}$	$\frac{m_4}{m_\infty}$	$\frac{A_3}{A_1}$
0.5	0.45	[a]1.0	0.483
.5	.41	[a].88	.435
.5	.41	.78	.382
.75	.43	[b].92	.445
1.0	.51	[a].91	.428
1.0	.44	[a].96	.395
1.5	.53	[a].91	.422
2.0	.57	.70	.343
2.0	.55	.70	.330
2.0	.55	.85	.379
3.0	.61	.74	.350
3.0	.58	.75	.343
4.0	.64	.40	.290
4.0	.58	.51	.340

(d) Fuselage I, diverter 1, figure 26(a)

AR	$\left(\frac{p_{t,4}}{p_{t,\infty}}\right)_{max}$	$\frac{m_4}{m_\infty}$	$\frac{A_3}{A_1}$
0.9	0.43	[a]0.69	0.475
1.8	.56	[b].81	.421
1.8	.52	.73	.382
1.8	.50	.72	.368
2.67	.52	[a].59	.375
2.67	.49	[a].97	.389
3.7	.56	[b].83	.313
3.7	.48	[b].80	.370

(e) Fuselage II, diverter 1, figure 26(b)

AR	$\left(\frac{p_{t,4}}{p_{t,\infty}}\right)_{max}$	$\frac{m_4}{m_\infty}$	$\frac{A_3}{A_1}$
[c]0.44	0.41	[a]0.99	0.497
.9	.44	[a].70	.475
1.8	.51	.82	.381
1.8	.50	[a].82	.420
2.6	.51	[a].84	.389
2.6	.47	.21	.375
3.7	.57	.85	.313
3.7	.48	[b].91	.367

(f) Fuselage III, diverter 1, figure 26(c)

AR	$\left(\frac{p_{t,4}}{p_{t,\infty}}\right)_{max}$	$\frac{m_4}{m_\infty}$	$\frac{A_3}{A_1}$
[c]0.44	0.41	0.89	0.497
[c].44	.40	[a]1.04	.552
[c].44	.37	.83	.436
.9	.45	.67	.475
1.8	.55	[b].64	.381
1.8	.54	.83	.370
1.8	.54	[a].74	.420
2.6	.59	[a].46	.389
2.6	.53	-----	.362
2.6	.53	[a].48	.362
3.7	.61	.14	.314
3.7	.54	[b].40	.368

[a]Started at low pressure recovery.

[b]Starting questionable.

[c]Bump diverter configuration.

TABLE I.- Concluded

TOTAL-PRESSURE RECOVERIES WITH CORRESPONDING MASS FLOW AND CONTRACTION RATIO

(g) Fuselage I, diverter 2, figure 27(a)

AR	$\left(\frac{p_{t,4}}{p_{t,\infty}}\right)_{max}$	$\frac{m_4}{m_\infty}$	$\frac{A_3}{A_1}$
0.67	0.38	[a]0.98	0.486
1.3	.49	.78	.378
1.3	.48	.77	.394
1.3	.47	[a].76	.420
1.8	.53	.75	.365
1.8	.51	.76	.352
2.67	.55	.86	.366
2.67	.54	[b].71	.344
3.7	.54	.74	.322

(h) Fuselage II, diverter 2, figure 27(b)

AR	$\left(\frac{p_{t,4}}{p_{t,\infty}}\right)_{max}$	$\frac{m_4}{m_\infty}$	$\frac{A_3}{A_1}$
0.67	0.43	[a]0.97	0.486
.9	.46	.71	.390
1.35	.50	.80	.378
1.35	.48	.81	.394
1.35	.47	[a].81	.468
1.8	.55	.75	.313
1.8	.55	[a].81	.353
1.8	.53	.82	.365
1.8	.51	.77	.312
2.67	.53	[a].82	.344
2.67	.53	[b].81	.367
2.67	.51	.68	.293
2.67	.51	.63	.267
3.70	.58	.47	.297
3.70	.53	.75	.313
3.70	.52	.72	.287

(i) Fuselage III, diverter 2, figure 27(c)

AR	$\left(\frac{p_{t,4}}{p_{t,\infty}}\right)_{max}$	$\frac{m_4}{m_\infty}$	$\frac{A_3}{A_1}$
0.67	0.41	0.68	0.450
.67	.40	[a].97	.486
.9	.49	[a].97	.435
.9	.46	.74	.390
1.35	.54	.67	.378
1.35	.51	.69	.368
1.35	.50	[a].86	.394
1.35	.48	[a]1.00	.483
1.80	.57	.70	.352
1.80	.57	.57	.313
1.80	.55	[a].69	.365
1.80	.52	.56	.292
2.67	.60	.35	.344
2.67	.58	.40	.267
2.67	.58	.41	.293
2.67	.54	.74	.367
3.70	.67	[b].65	.313
3.70	.60	.34	.287
3.70	.59	.26	.297
3.70	.52	.32	.262

[a]Started at low pressure recovery.

[b]Starting questionable.

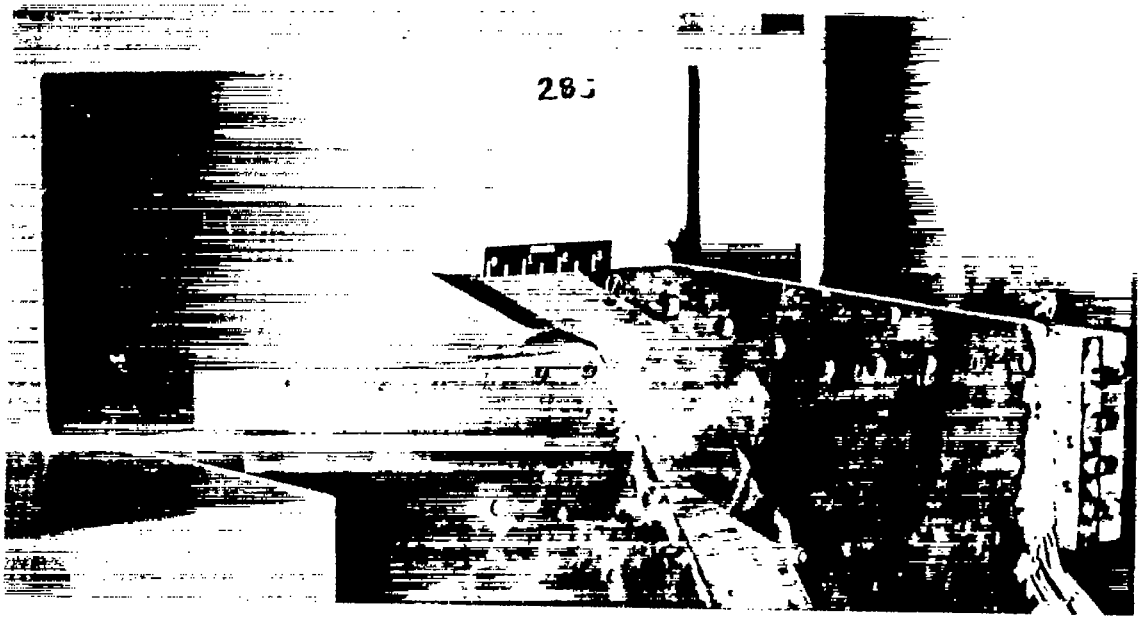

(a) With inlet side walls. L-57-333

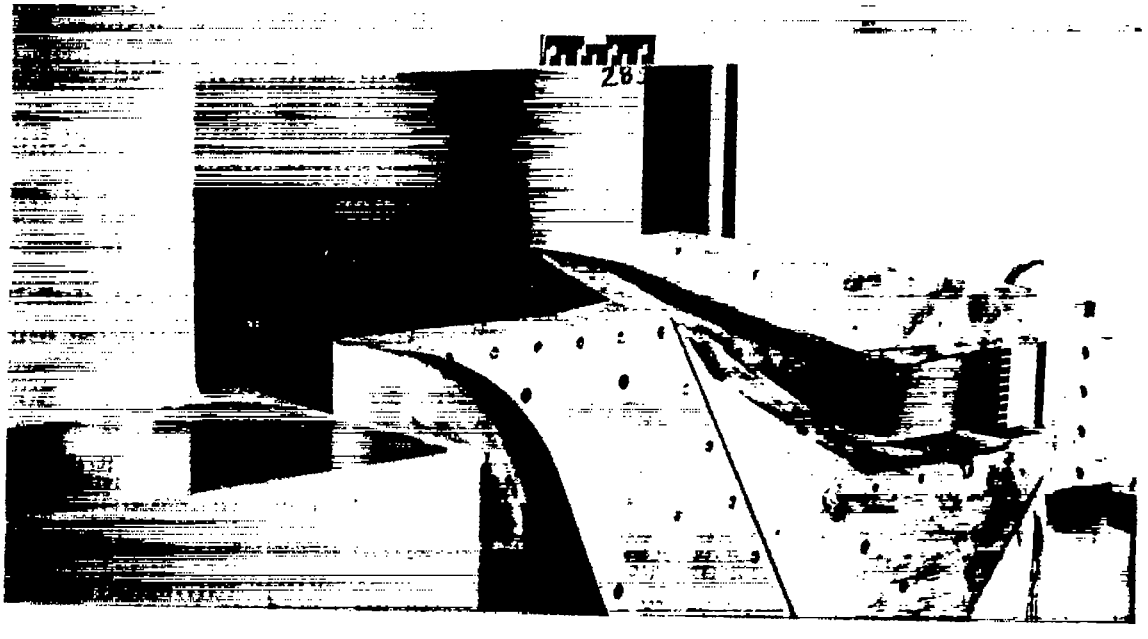

(b) Internal contours exposed. L-57-335

Figure 1.- Photographs of inlet model. AR = 1.0; fuselage III; boundary-layer diverter 2.

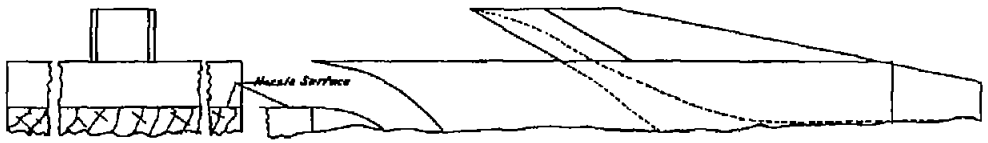

(a) Fuselage I, fuselage width equal to tunnel width.

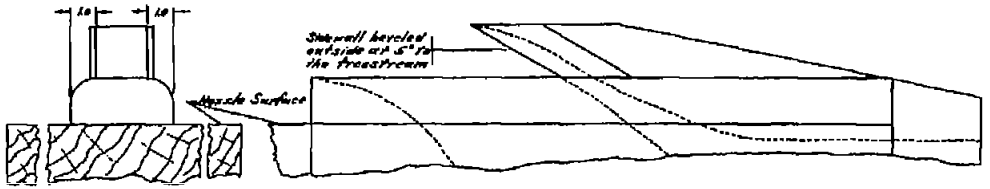

(b) Fuselage II, fuselage 2 inches wider than inlet.

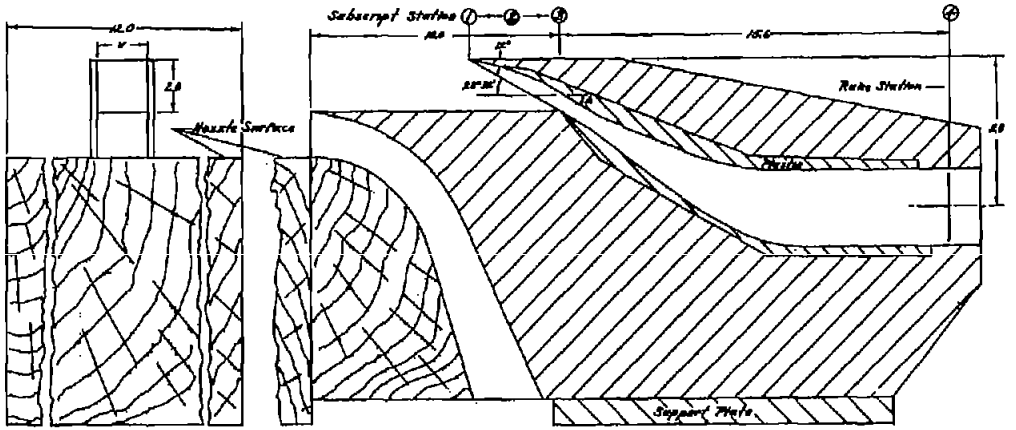

(c) Fuselage III, fuselage width equal to inlet width, internal surfaces exposed.

Figure 2.- Schematic drawing of inlet.

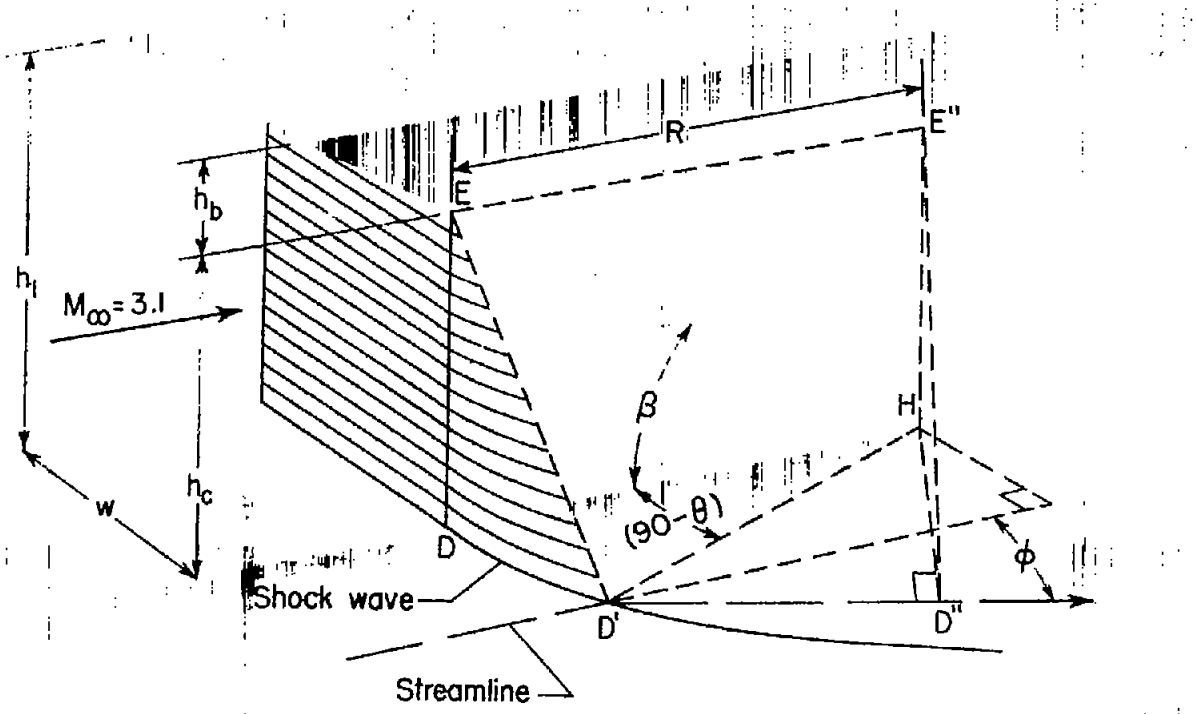

(a) Three-dimensional view of assumed shock-wave configuration.

Figure 3.- Flow model assumed for approximate theory of starting.

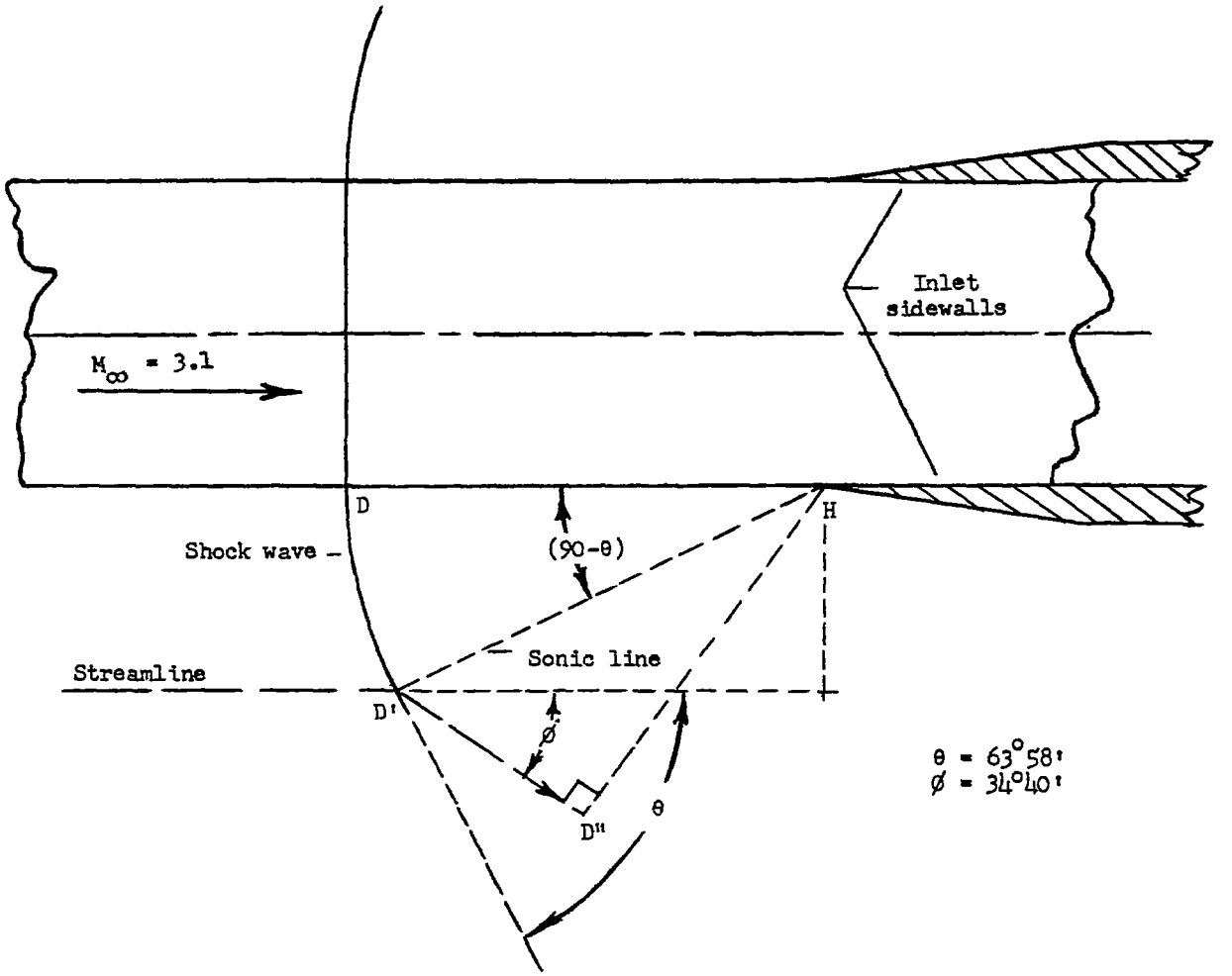

(b) Two-dimensional view in a plane parallel to free stream and normal to inlet side walls of assumed shock wave at a particular position.

Figure 3.- Concluded.

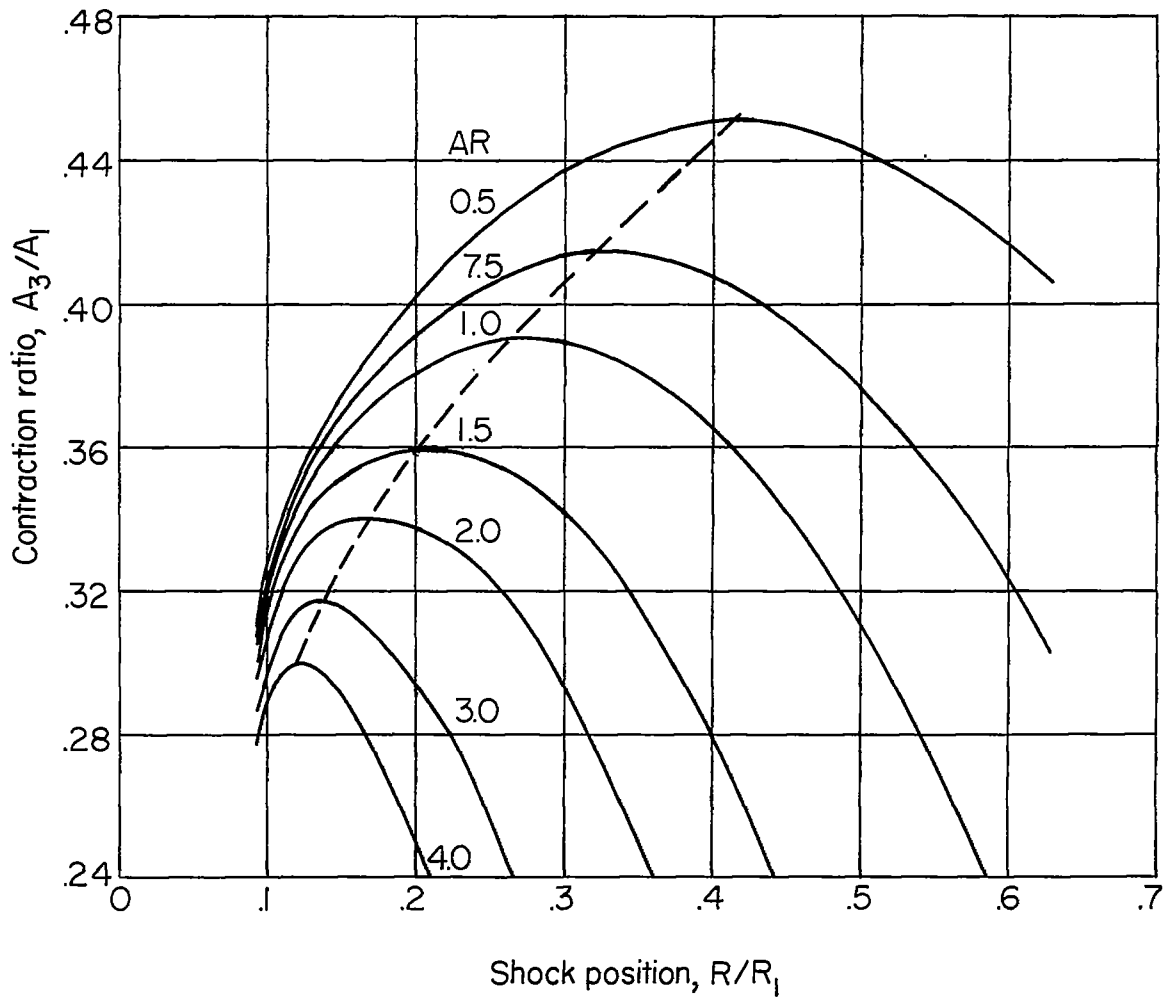

Figure 4.- Variation of required inlet contraction ratio with assumed shock-wave position relative to the inboard inlet lip for inlets of various aspect ratios. $M_\infty = 3.1$; $\beta = 28^\circ 32'$.

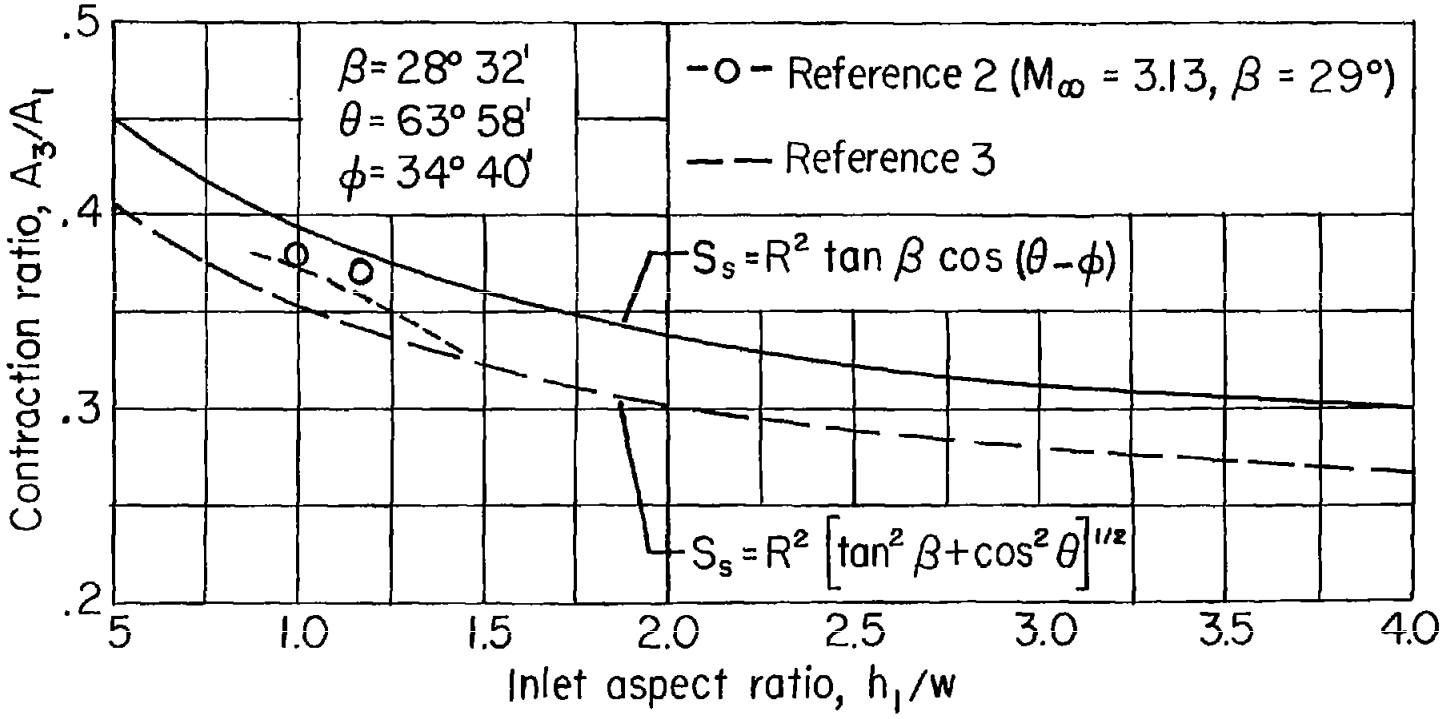

Figure 5.- Theoretical variation of starting minimum inlet contraction ratio with inlet aspect ratio and comparison with references 2 and 3. $M_\infty = 3.1$.

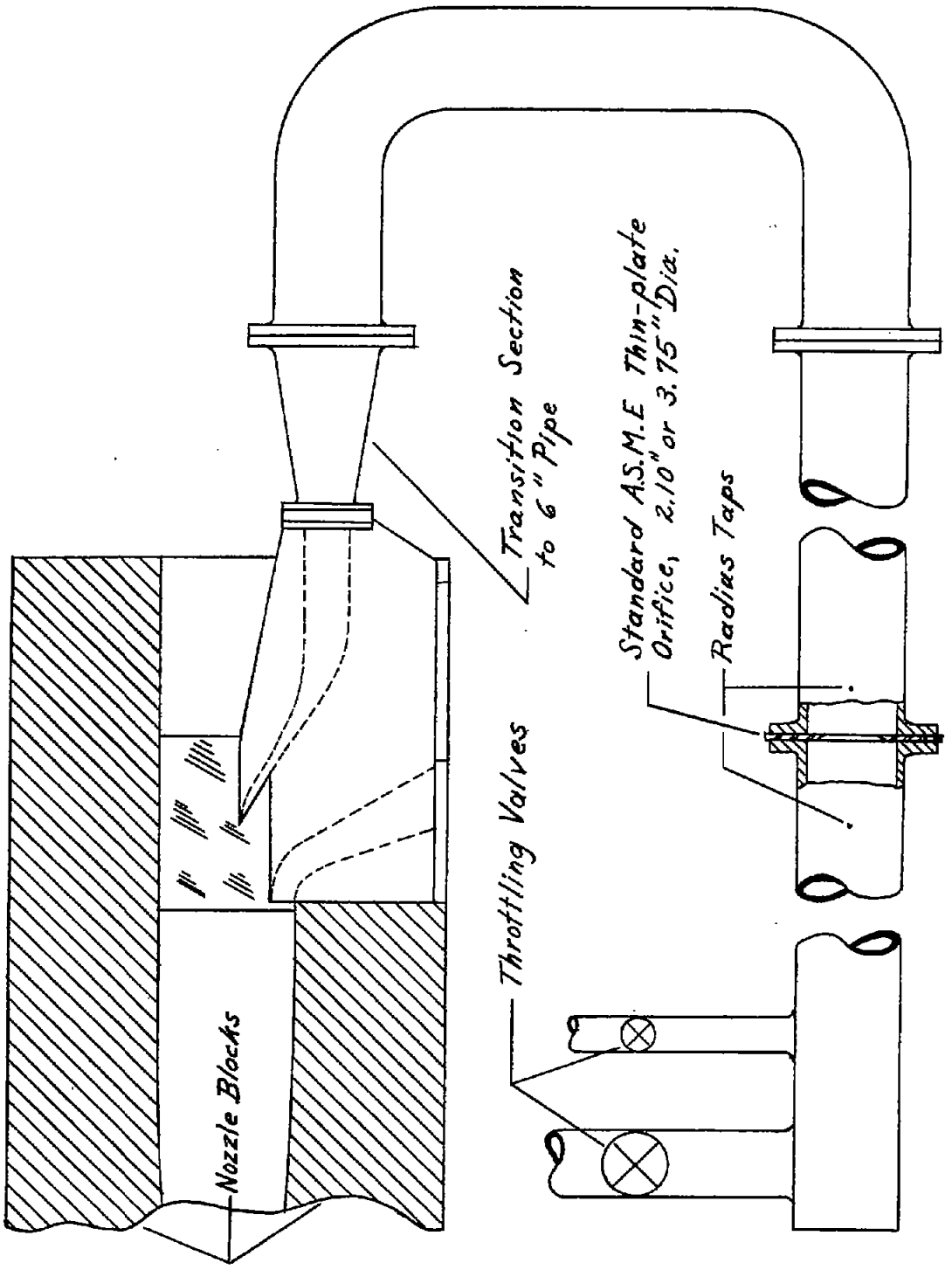

Figure 6.- Schematic drawing of test installation.

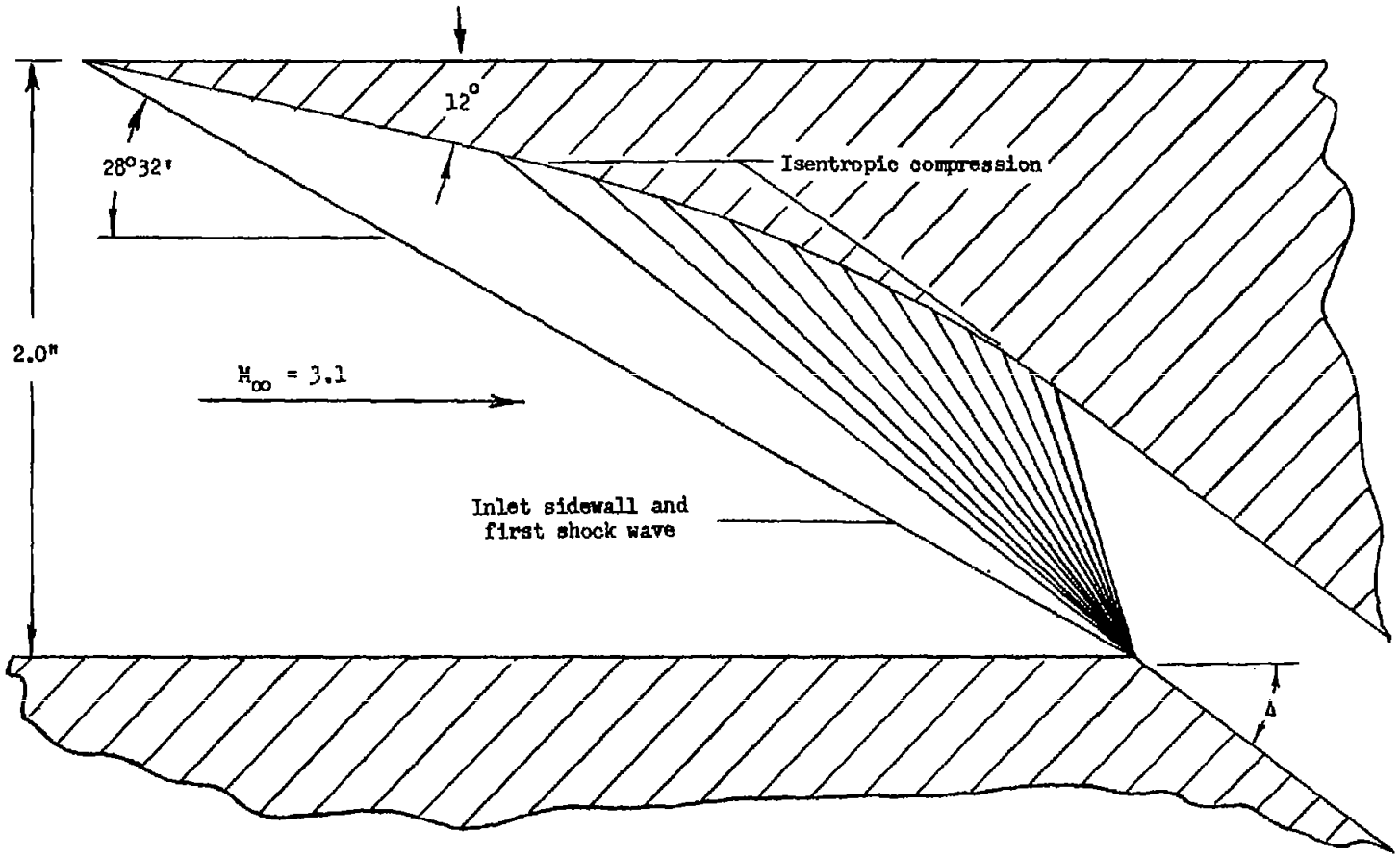

Figure 7.- Inlet design shock-wave system. $M_\infty = 3.1$.

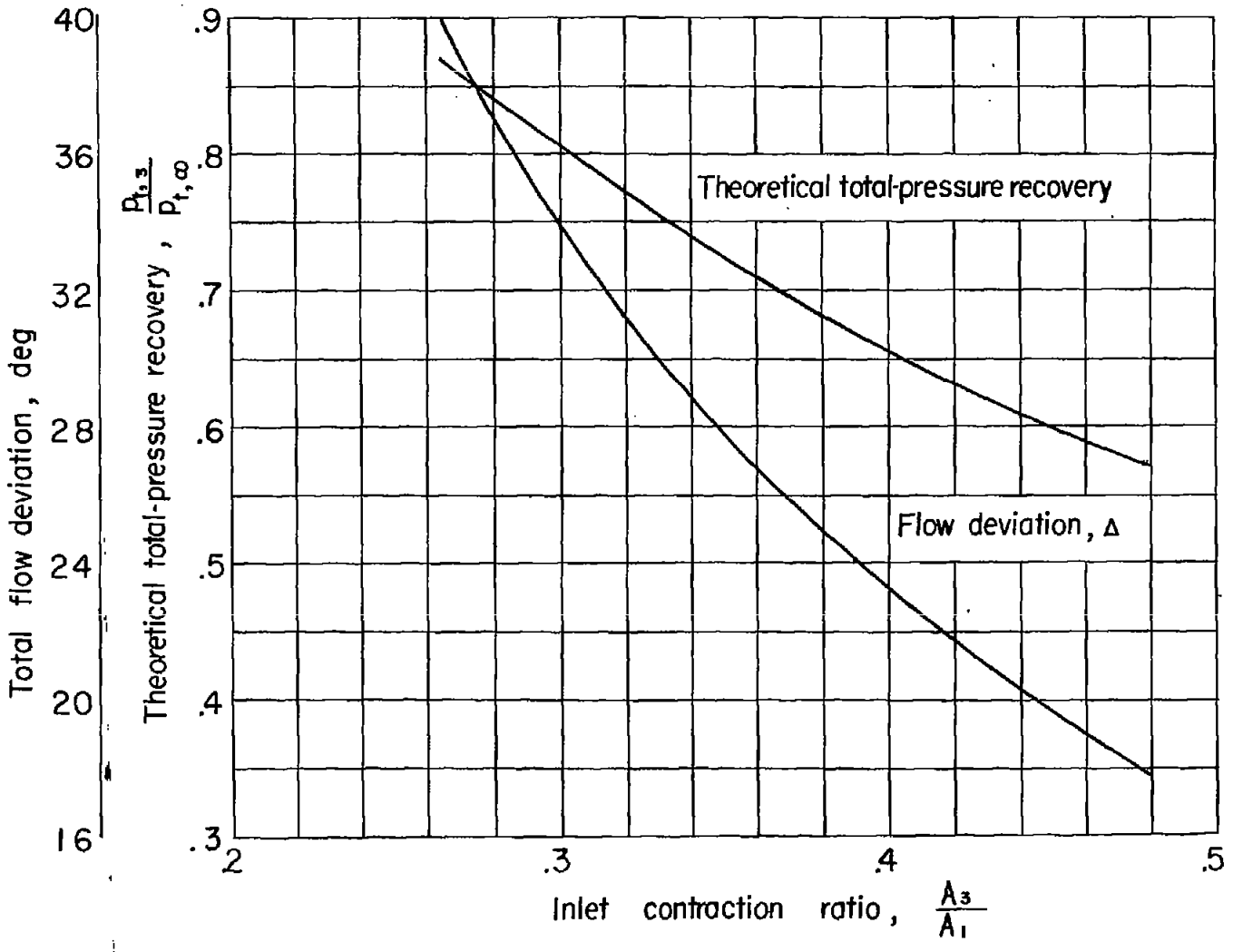

Figure 8.- Variation of total flow deviation and theoretical total-pressure recovery with inlet contraction ratio. $M_\infty = 3.1$.

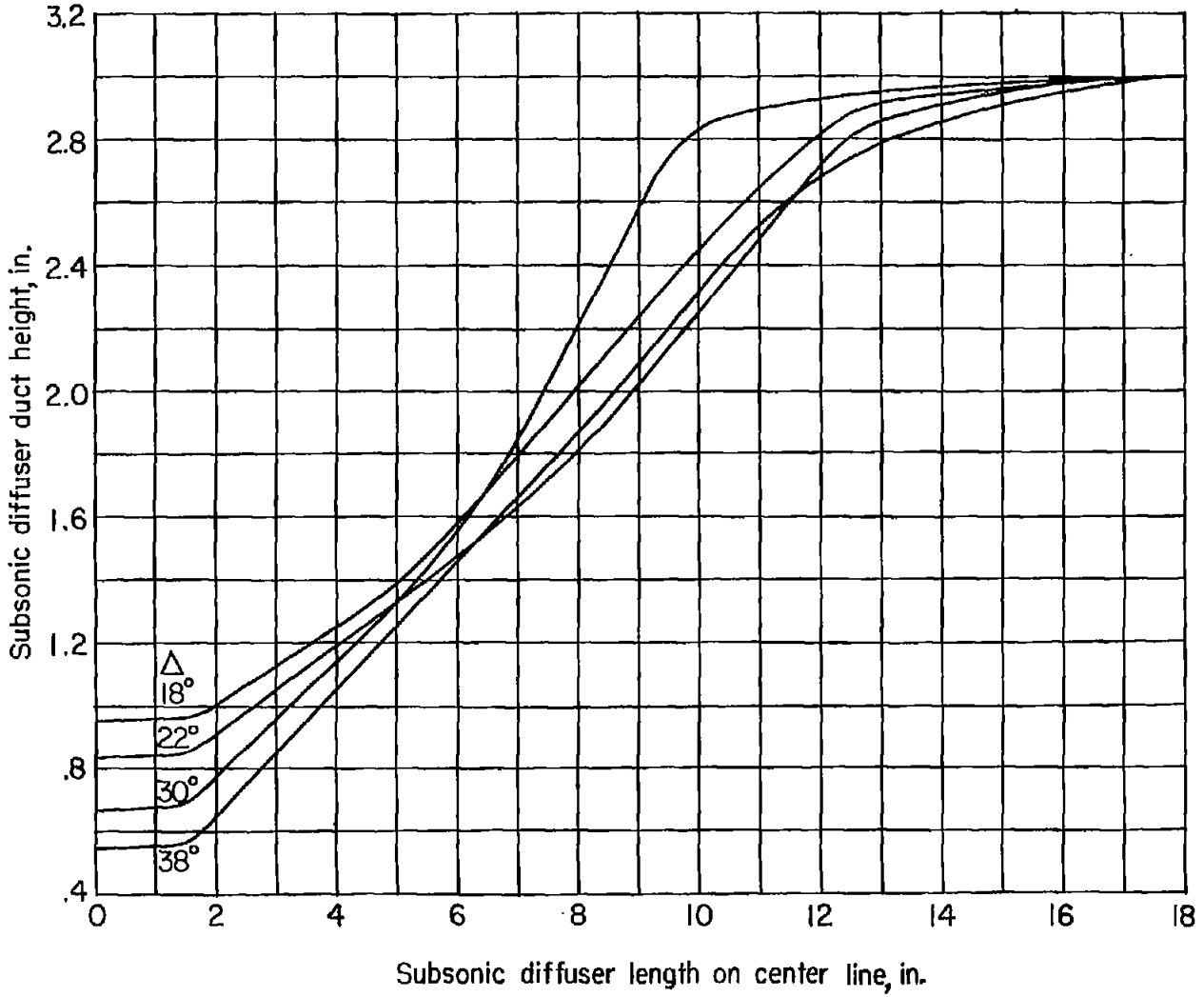

Figure 9.- Variation of subsonic duct height with length on duct center line for various amounts of total-flow deviation Δ.

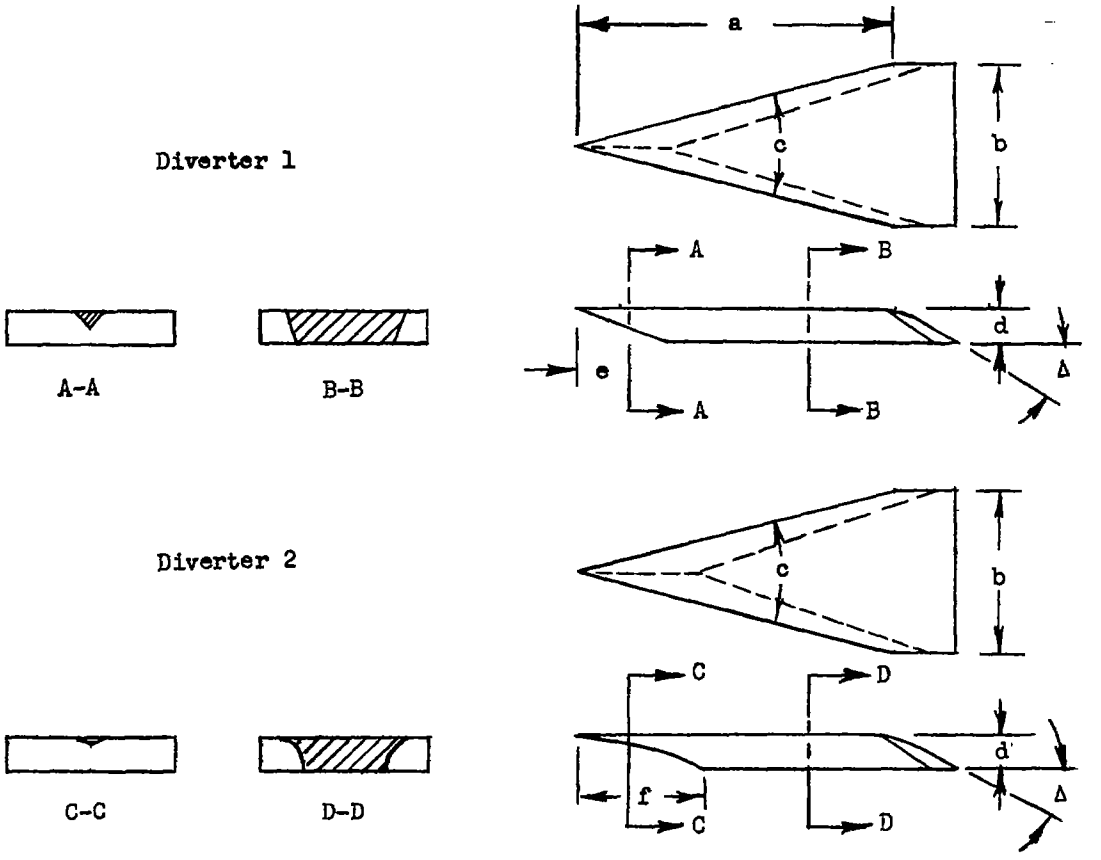

Nominal AR	Effective AR	Diverters 1 and 2				Div. 1	Div. 2
		a	b	c(deg.)	d	e	f
0.5	0.44	4.83	4.00	45	0.25	0.69	
0.75	0.67	3.22	2.67	45	0.20	0.55	1.00
1.0	0.90	2.75	2.00	40	0.20	0.55	1.12
1.5	1.35	2.49	1.33	30	0.20	0.55	1.10
2.0	1.80	1.87	1.00	30	0.20	0.55	0.65
3.0	2.67	1.25	0.67	30	0.20	0.55	0.53
4.0	3.70	0.93	0.50	30	0.15	0.41	0.48

(a) Wedge diverters 1 and 2.

Figure 10.- Boundary-layer diverter details. All dimensions are in inches.

[redacted]

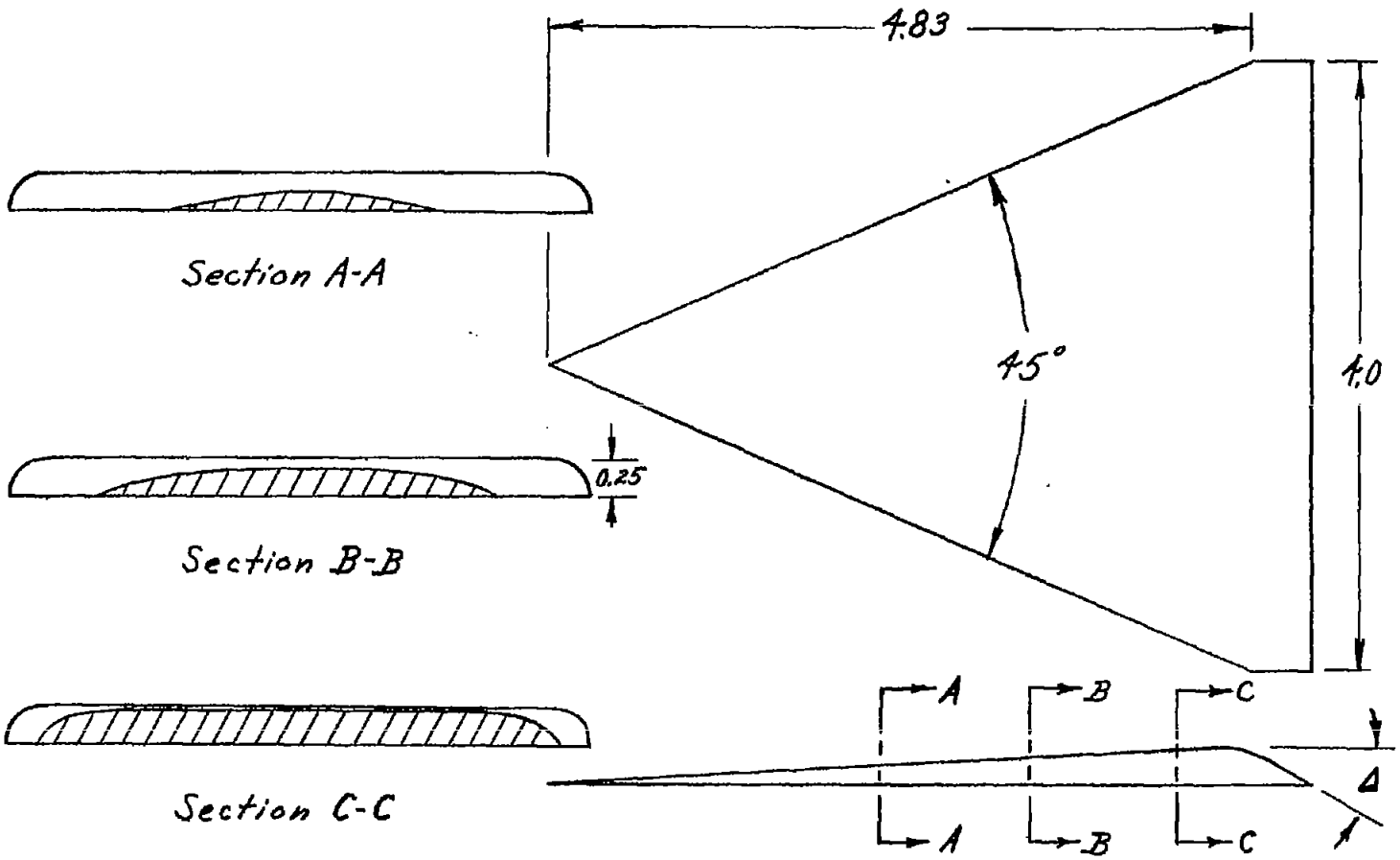

(b) Bump diverter for aspect-ratio-0.5 inlet.

Figure 10.- Concluded.

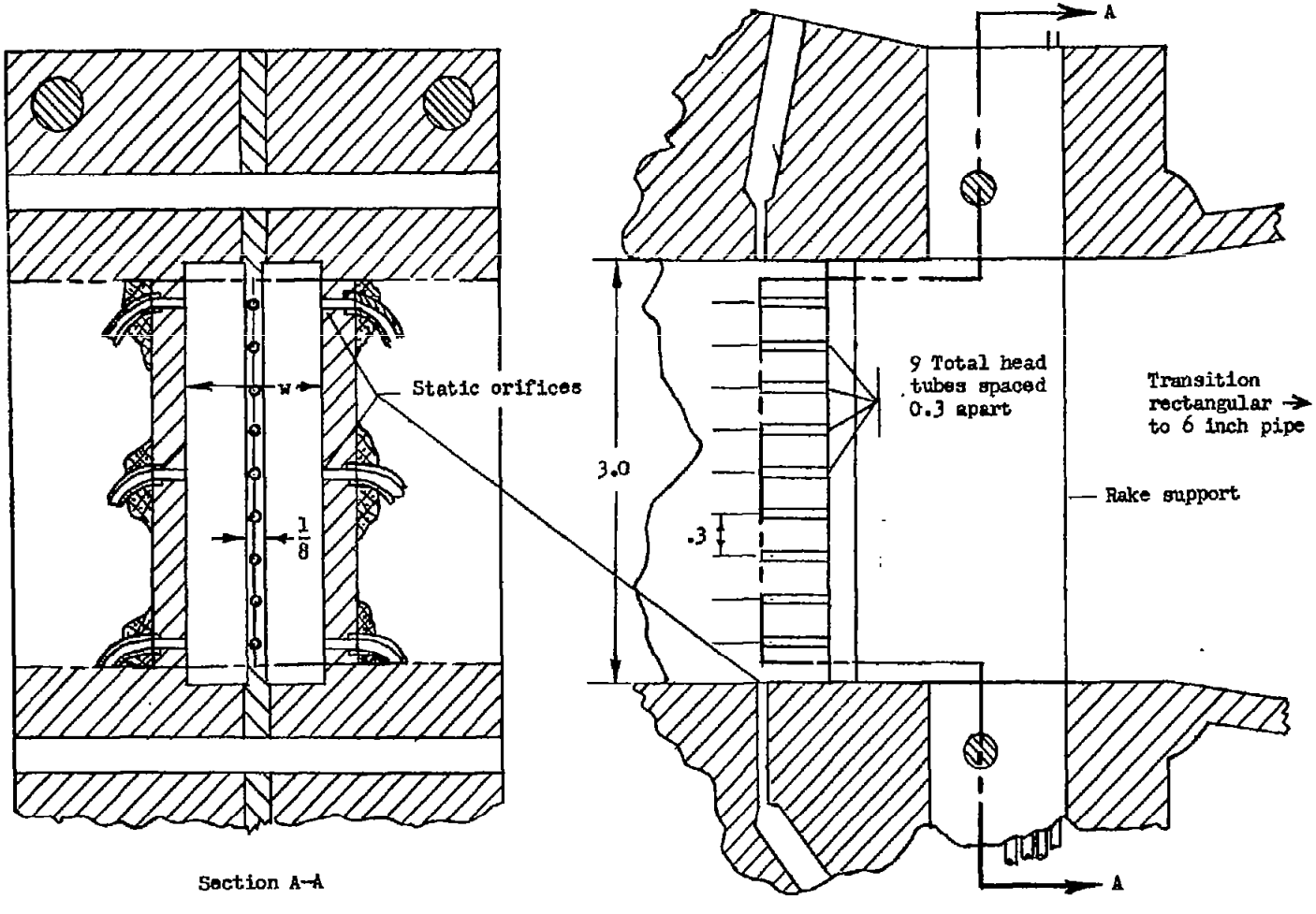

Figure 11.- Details of total-pressure rake and static-orifice locations at diffuser exit. All dimensions are in inches.

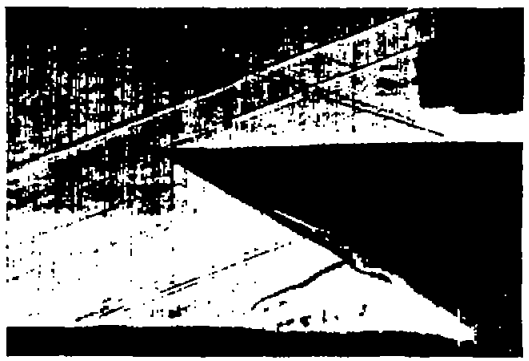

(a) No diverter; AR = 2.0; A_3/A_1 = 0.314; $\left(m_4/m_\infty\right)_{max}$ = 0.82.

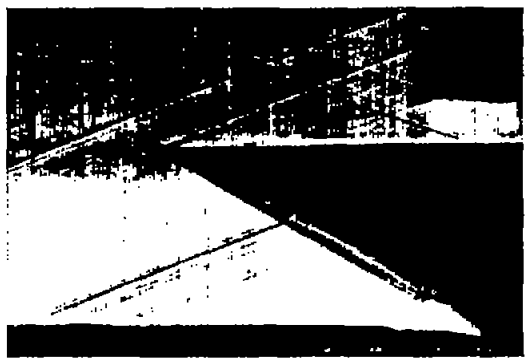

(b) No diverter; AR = 2.0; A_3/A_1 = 0.343; $\left(m_4/m_\infty\right)_{max}$ = 0.92.

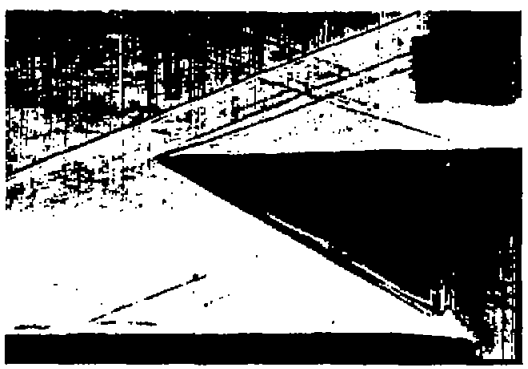

(c) No diverter; AR = 2.0; A_3/A_1 = 0.394; $\left(m_4/m_\infty\right)_{max}$ = 0.98.

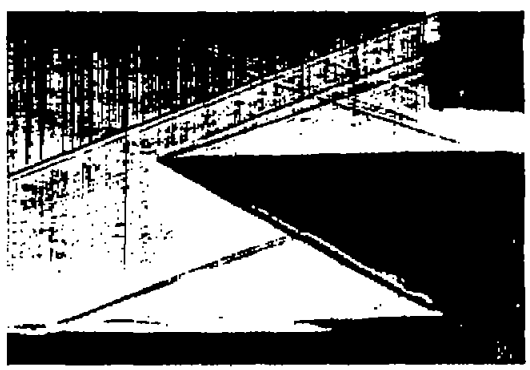

(d) Diverter 2; AR = 1.8; A_3/A_1 = 0.420; $\left(m_4/m_\infty\right)_{max}$ = 0.98.

L-57-2757

Figure 12.- Typical shadow photographs of inlets, started and not started, of varying contraction ratio. Fuselage II; M_∞ = 3.1.

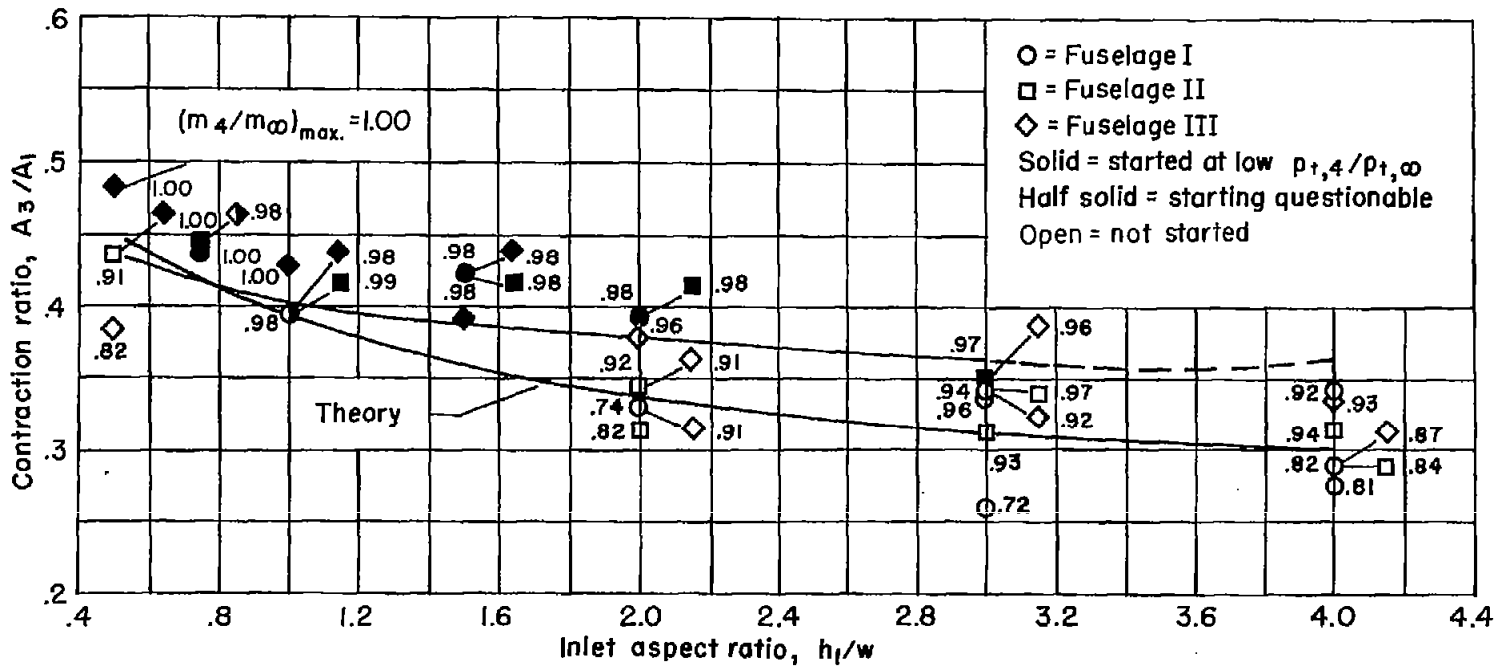

Figure 13.- Effect of inlet aspect ratio on the minimum starting inlet contraction ratio with no boundary-layer diversion. $M_\infty = 3.1$.

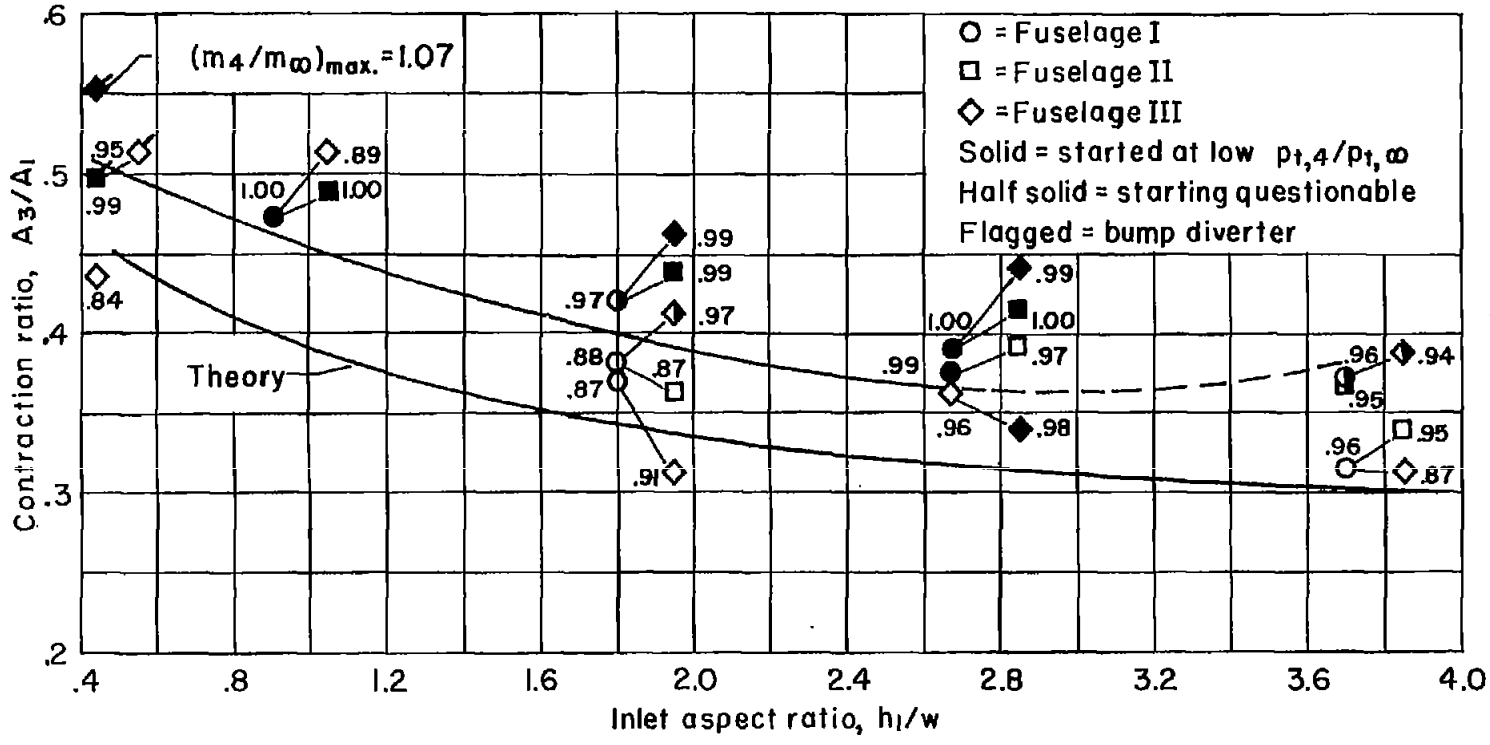

Figure 14.- Effect of inlet aspect ratio on the minimum starting inlet contraction ratio with boundary-layer diversion. Diverter 1; M_∞ = 3.1.

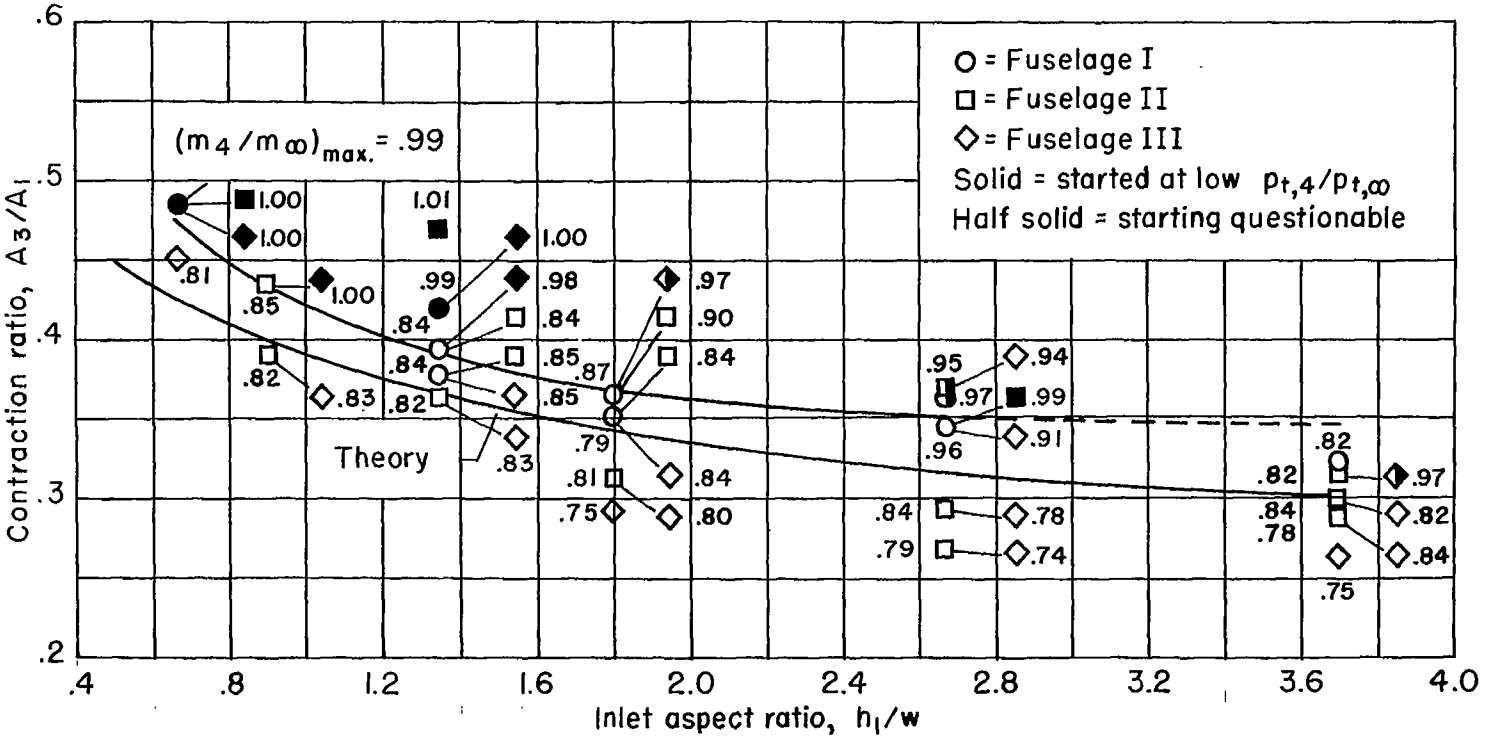

Figure 15.- Effect of inlet aspect ratio on the minimum starting inlet contraction ratio with boundary-layer diversion. Diverter 2; M_∞ = 3.1.

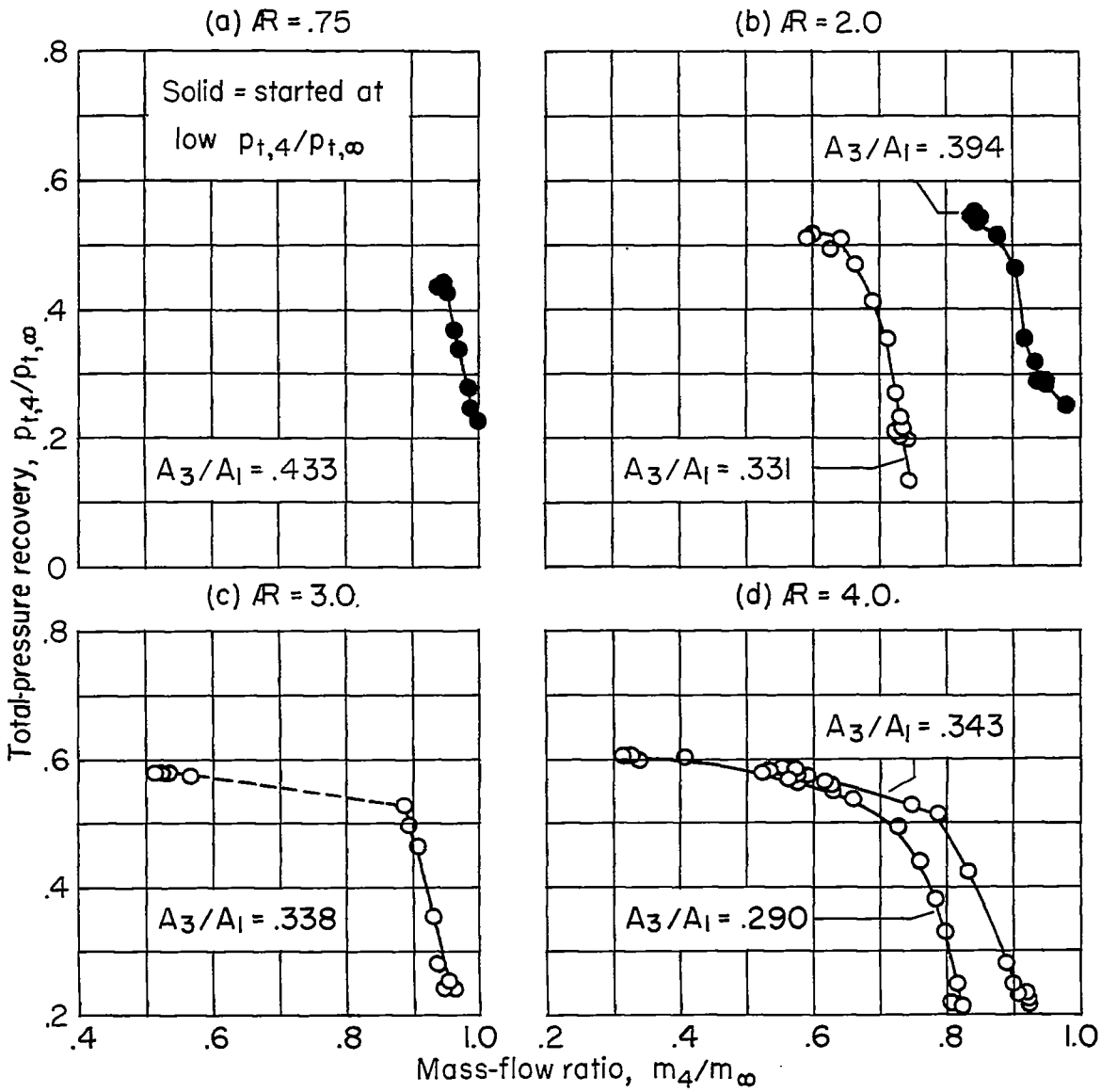

Figure 16.- Typical total-pressure-recovery variation with mass-flow ratio for fuselage I, no boundary-layer diversion, and various contraction ratios resulting in started or not-started configurations. M_∞ = 3.1.

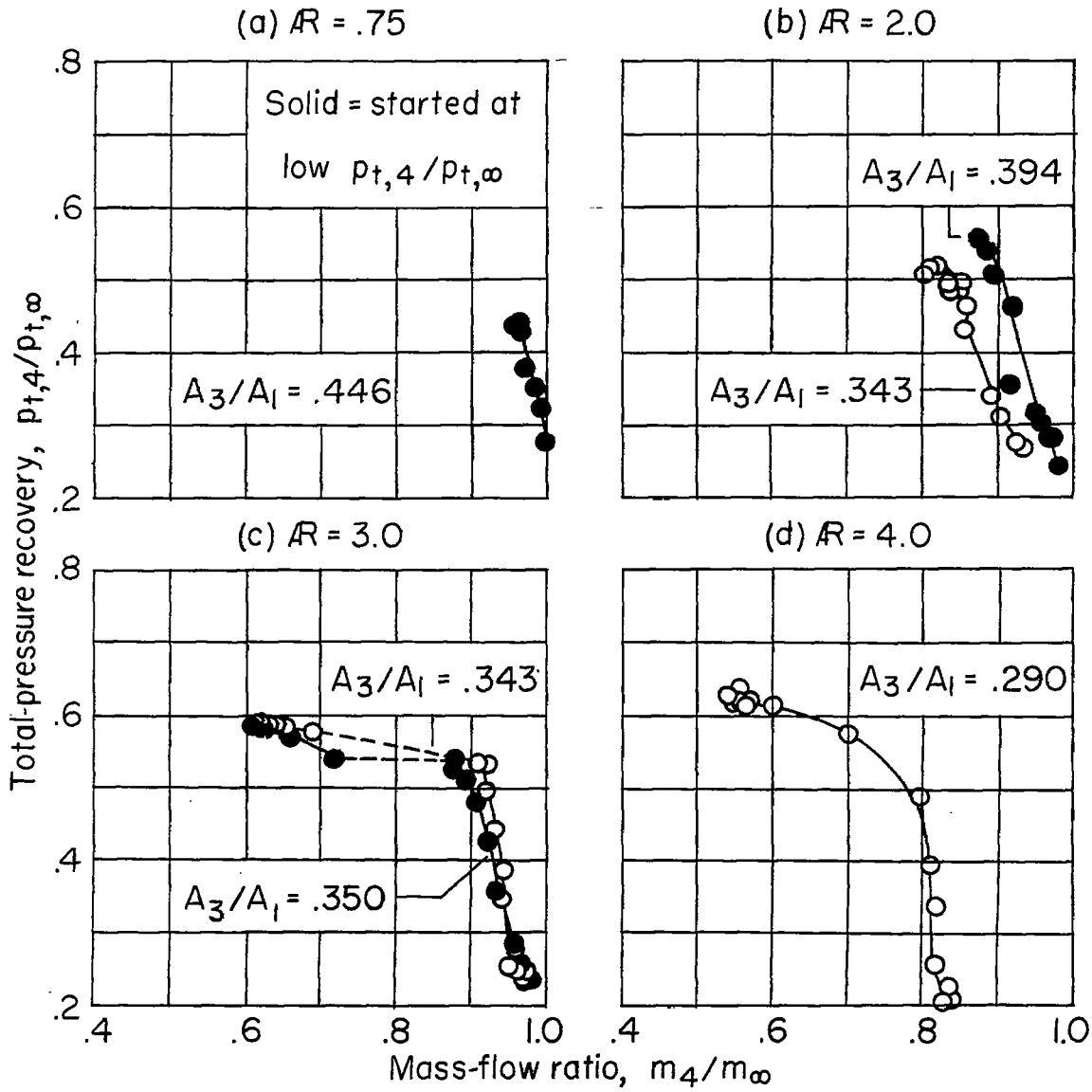

Figure 17.- Typical total-pressure-recovery variation with mass-flow ratio for fuselage II, no boundary-layer diversion, and various contraction ratios resulting in started or not-started configurations. M_∞ = 3.1.

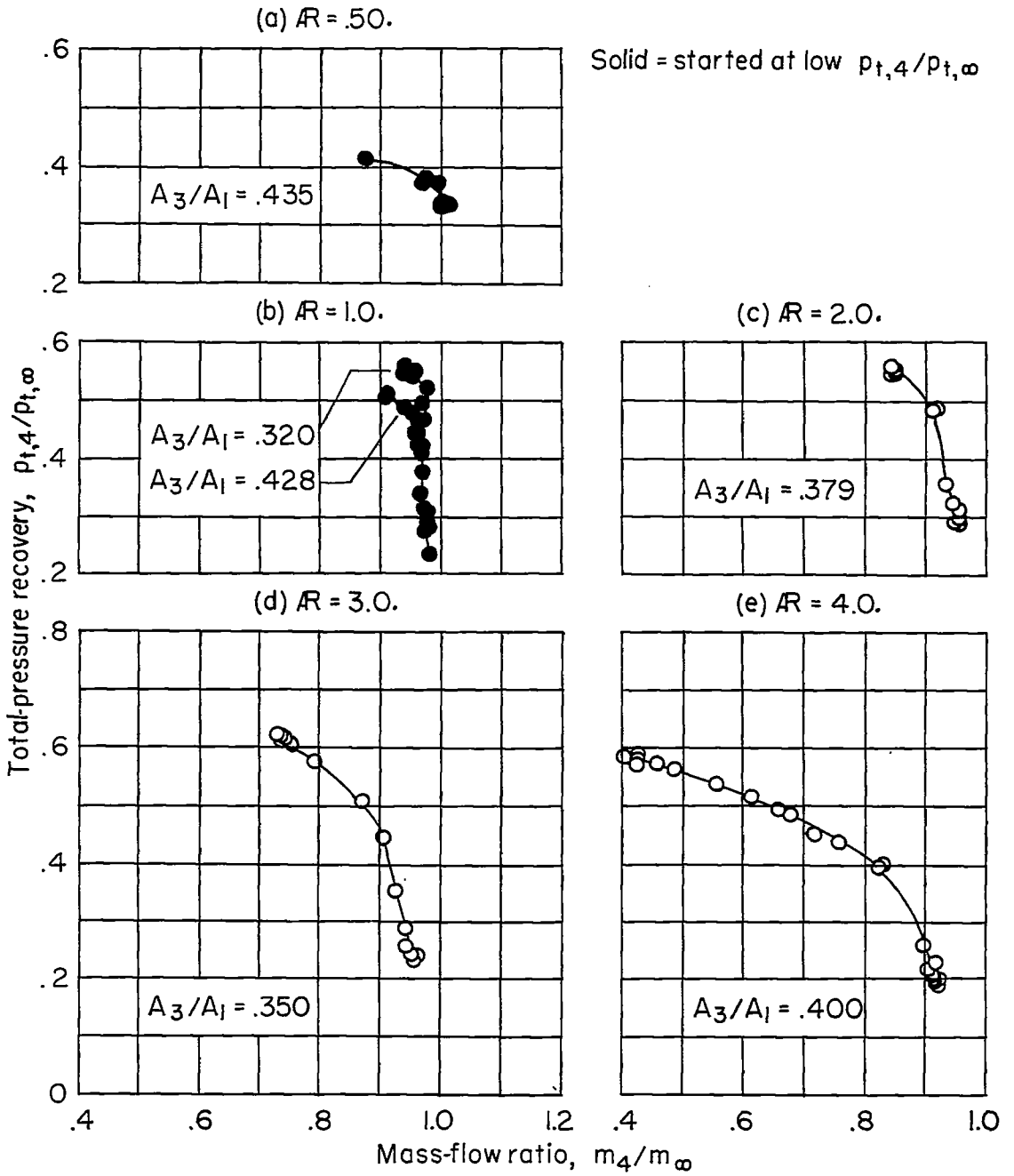

Figure 18.- Typical total-pressure-recovery variation with mass-flow ratio for fuselage III, no boundary-layer diversion, and various contraction ratios resulting in started or not-started configurations. M_∞ = 3.1.

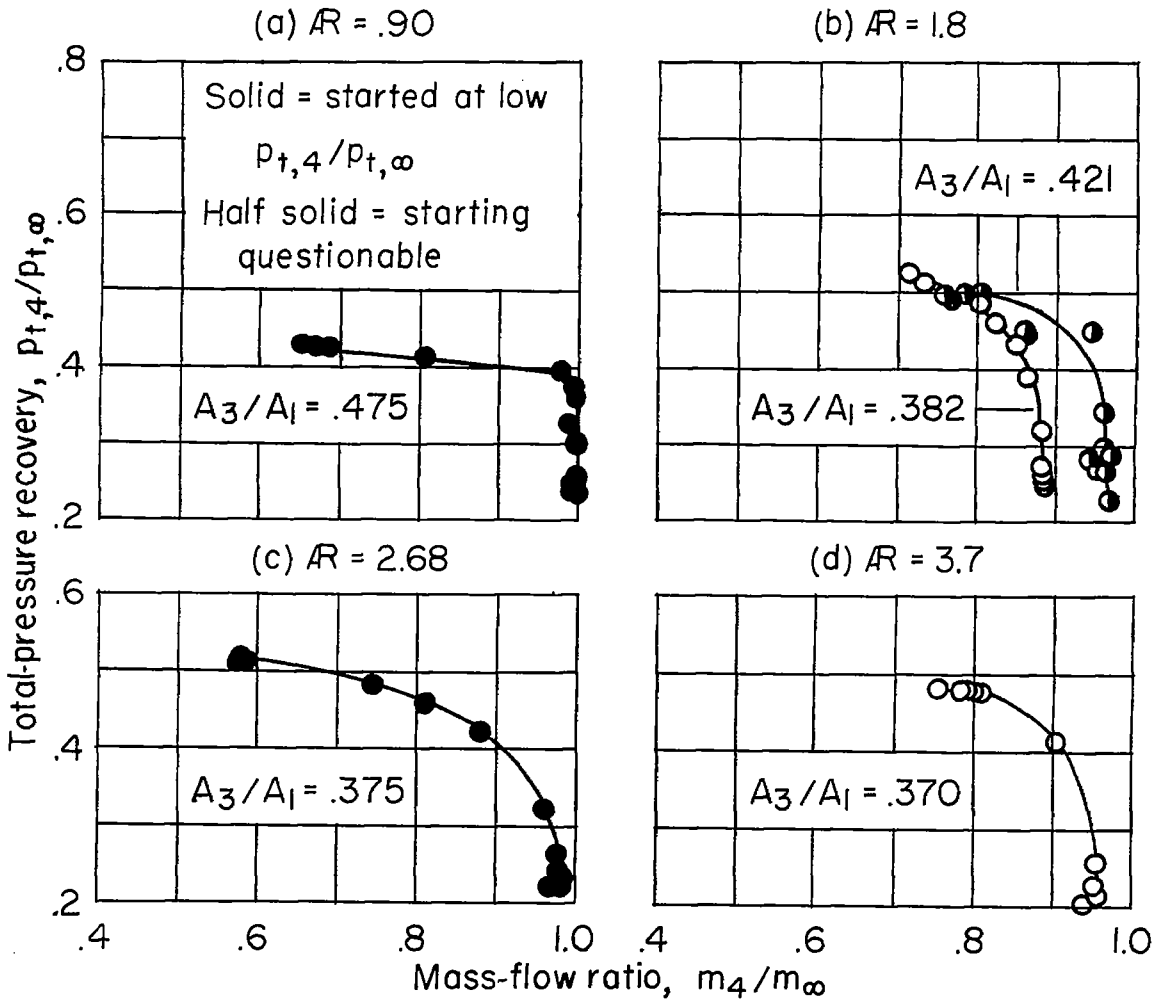

Figure 19.- Typical total-pressure-recovery variation with mass-flow ratio for fuselage I, diverter 1, and various contraction ratios resulting in started or not-started configurations. M_∞ = 3.1.

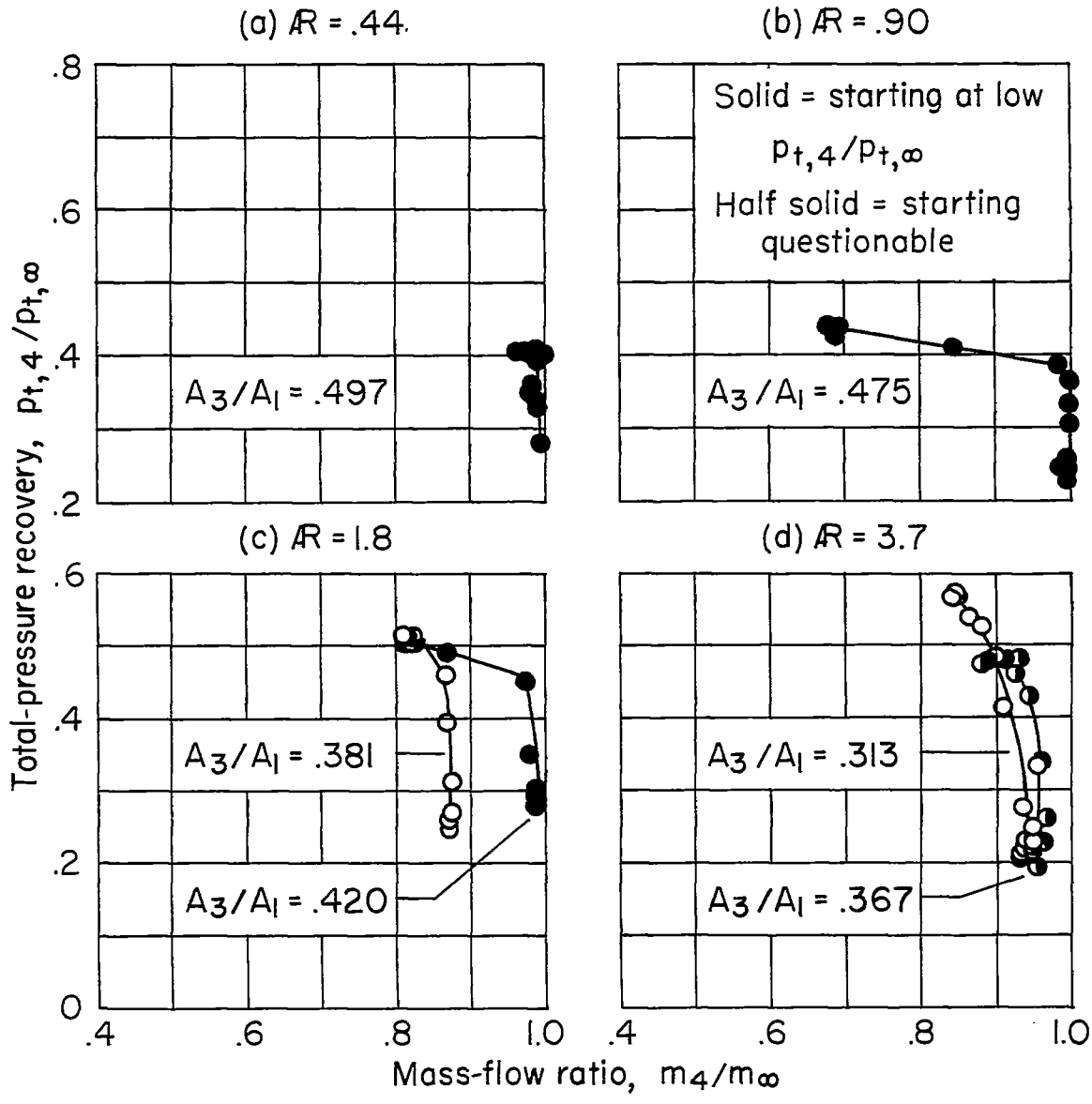

Figure 20.- Typical total-pressure-recovery variation with mass-flow ratio for fuselage II, diverter 1, and various contraction ratios resulting in started or not-started configurations. M_∞ = 3.1.

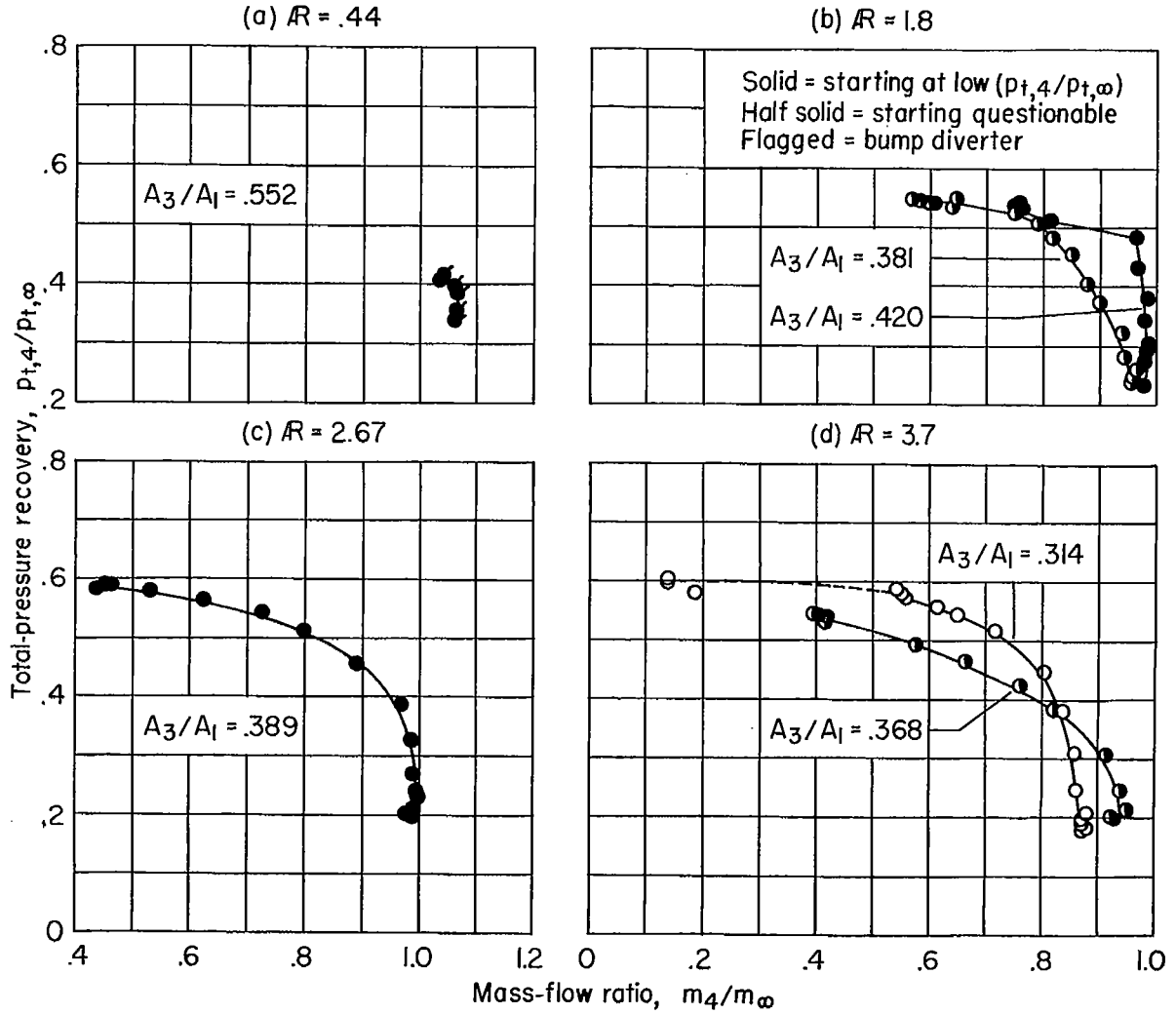

Figure 21.- Typical total-pressure-recovery variation with mass-flow ratio for fuselage III, diverter 1, and various contraction ratios resulting in started or not-started configurations. M_∞ = 3.1.

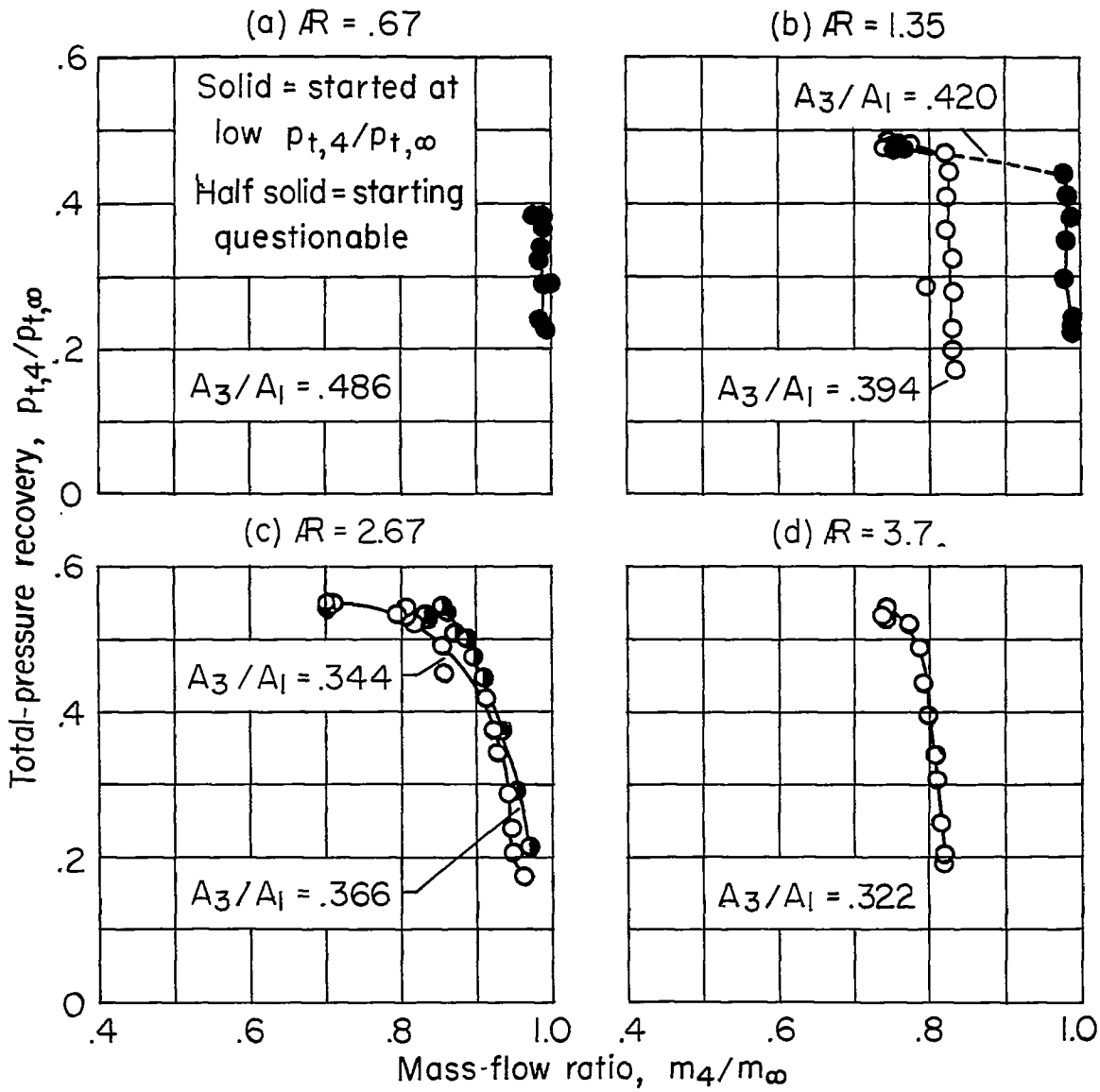

Figure 22.- Typical total-pressure-recovery variation with mass-flow ratio for fuselage I, diverter 2, and various contraction ratios resulting in started or not-started configurations. M_∞ = 3.1.

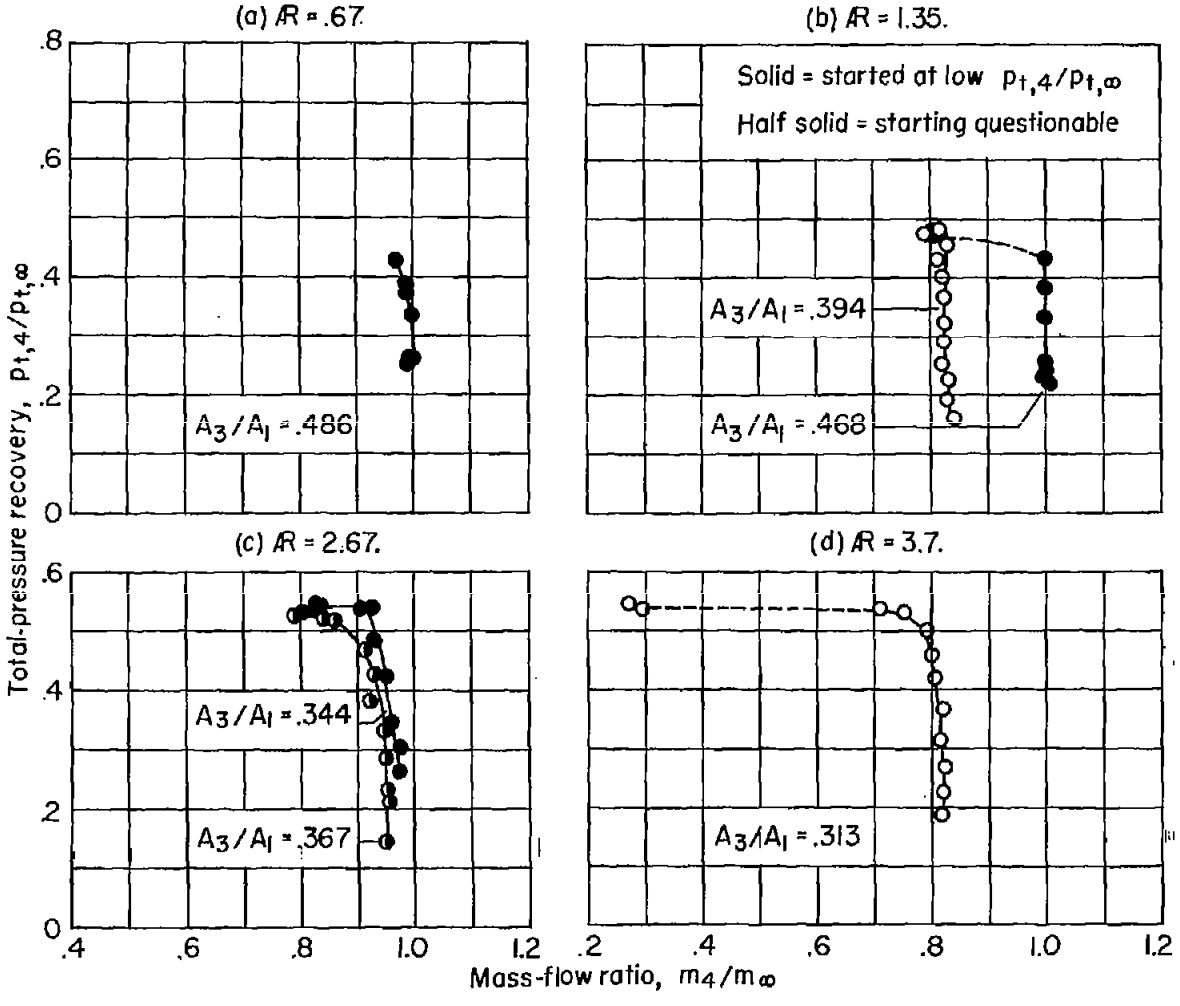

Figure 23.- Typical total-pressure-recovery variation with mass-flow ratio for fuselage II, diverter 2, and various contraction ratios resulting in started or not-started configurations. M_∞ = 3.1.

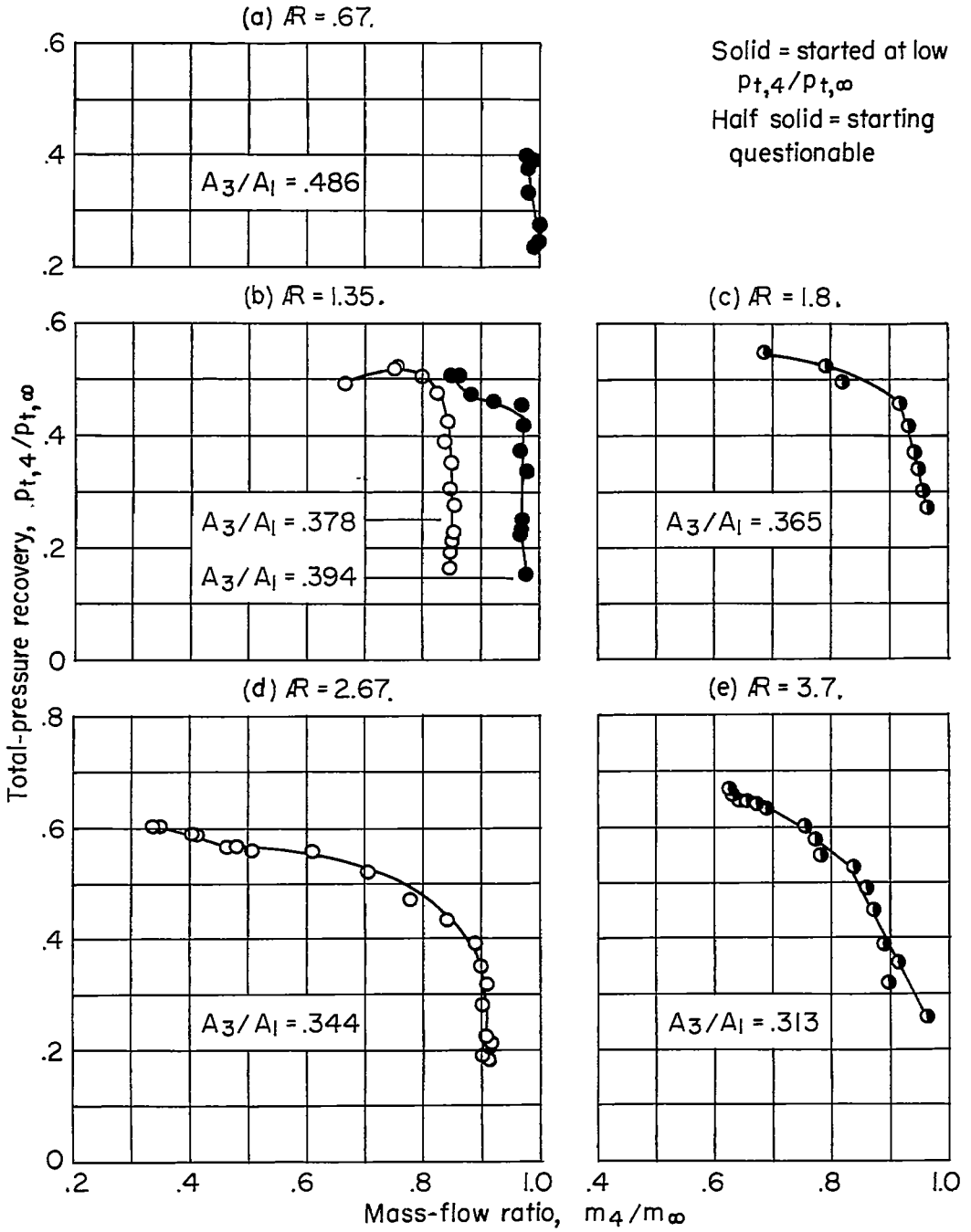

Figure 24.- Typical total-pressure-recovery variation with mass-flow ratio for fuselage III, diverter 2, and various contraction ratios resulting in started or not-started configurations. M_∞ = 3.1.

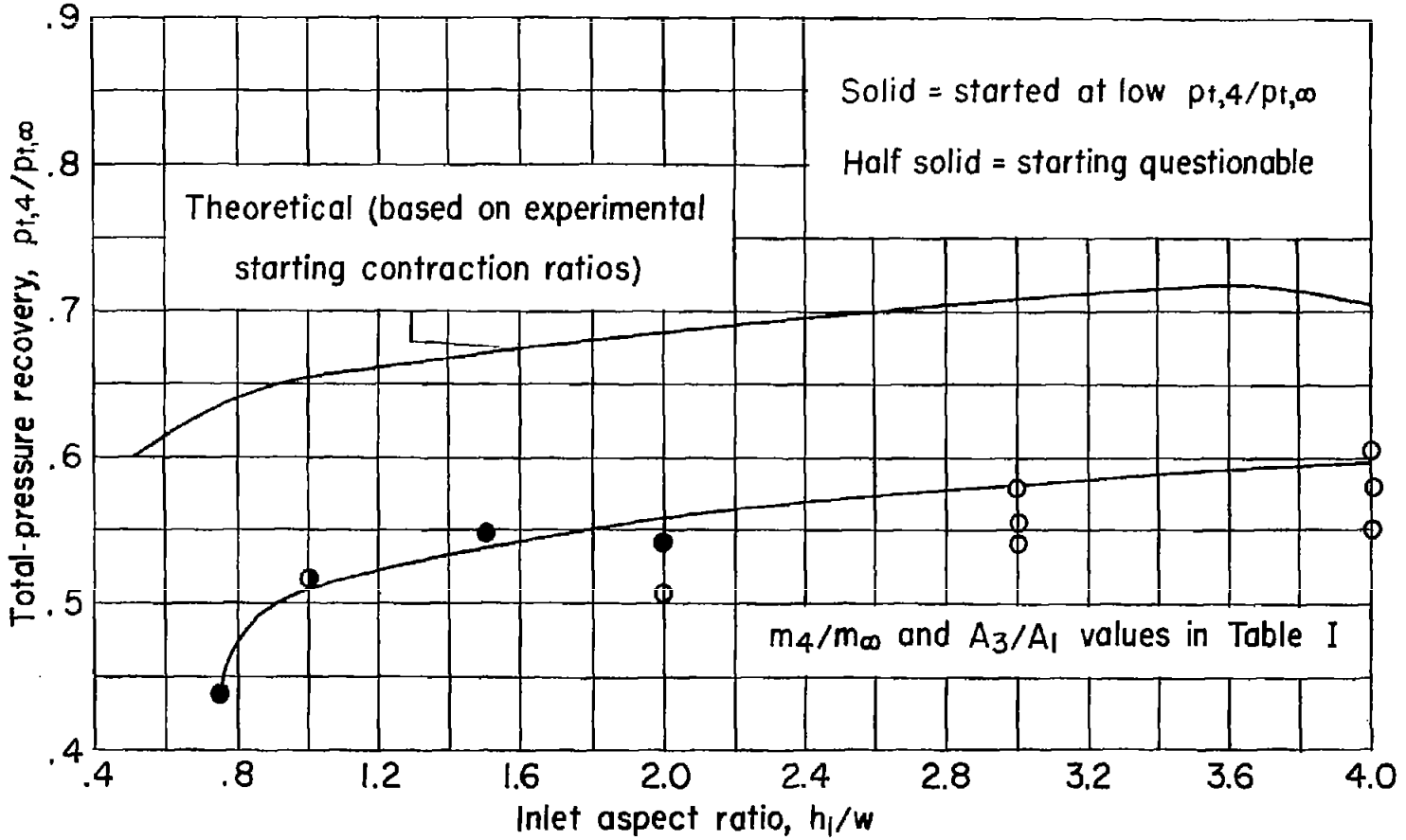

Figure 25.- Effect of inlet aspect ratio on the maximum total-pressure recovery with no boundary-layer diversion. $M_\infty = 3.1$.

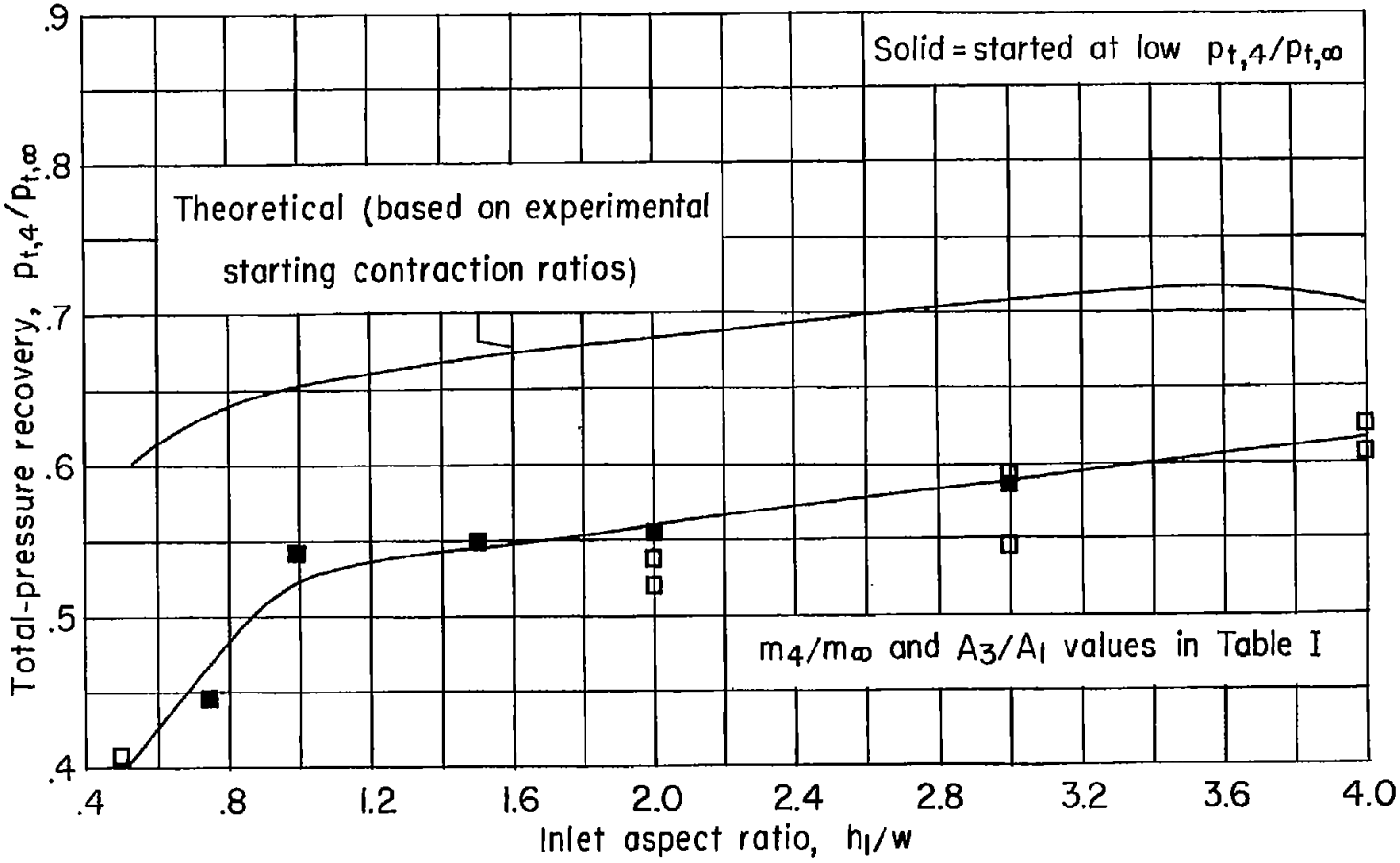

Figure 25.- Continued.

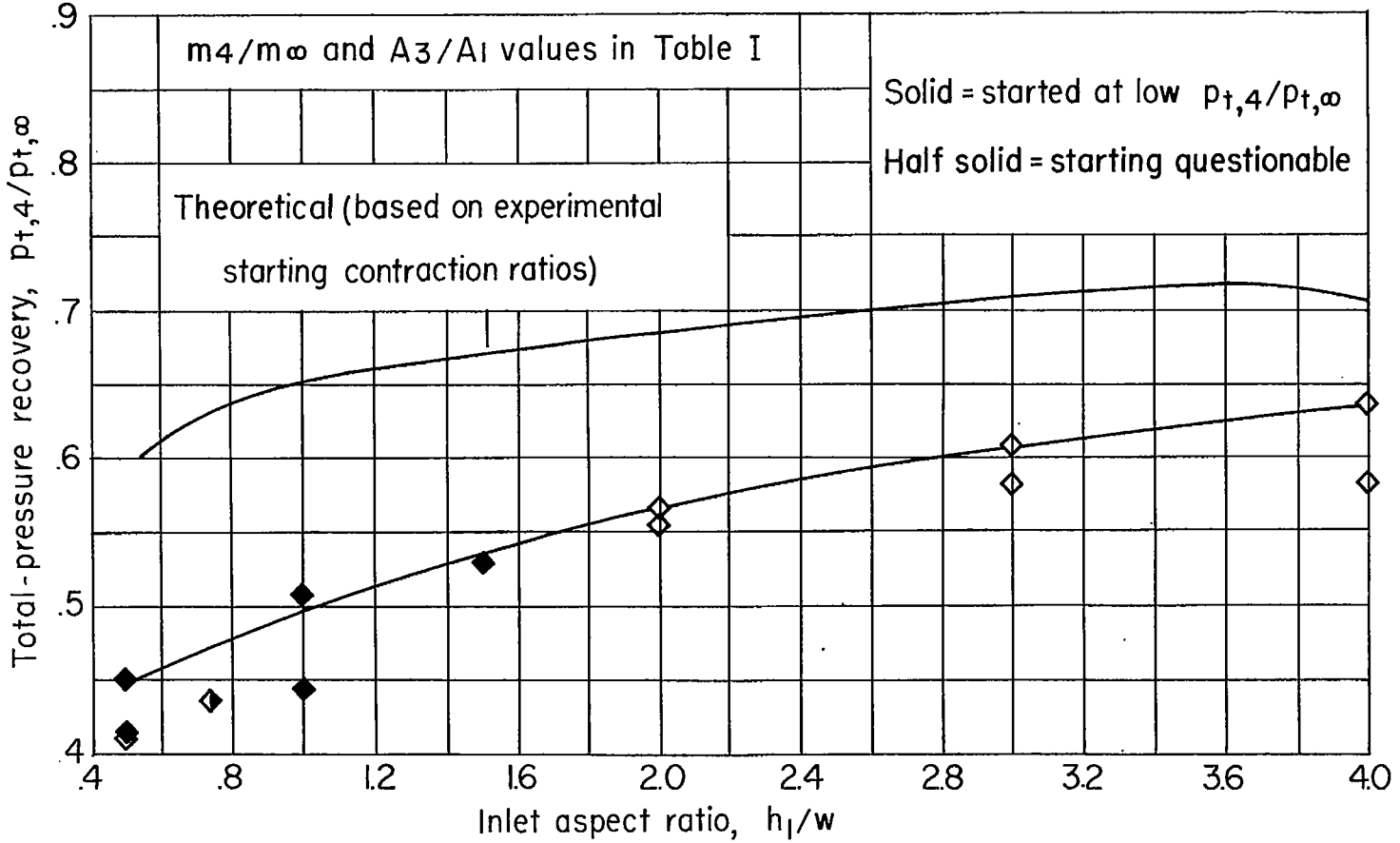

Figure 25.- Concluded.

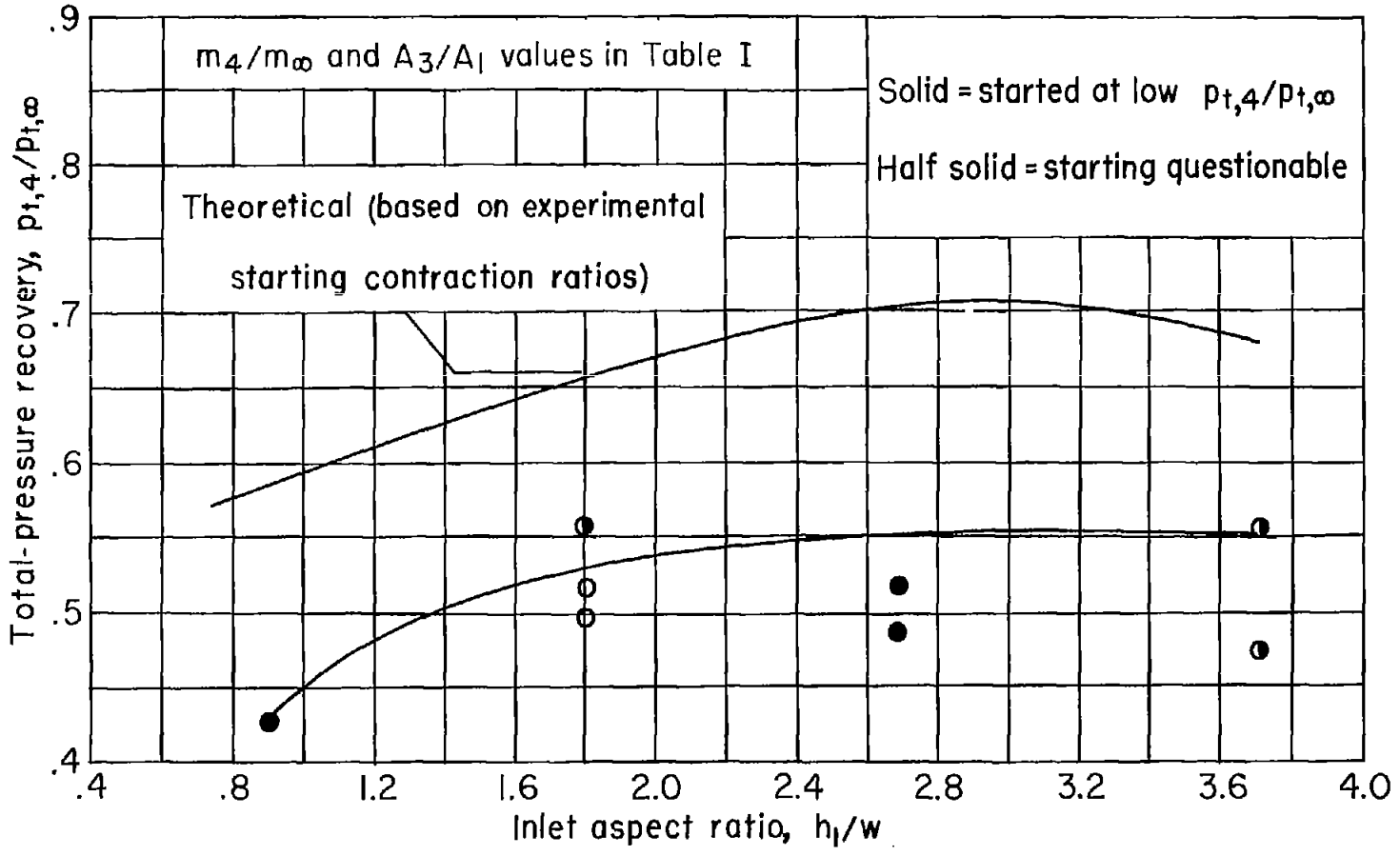

Figure 26.- Effect of inlet aspect ratio on the maximum total-pressure recovery with no boundary-layer diversion. Diverter 1; $M_\infty = 3.1$.

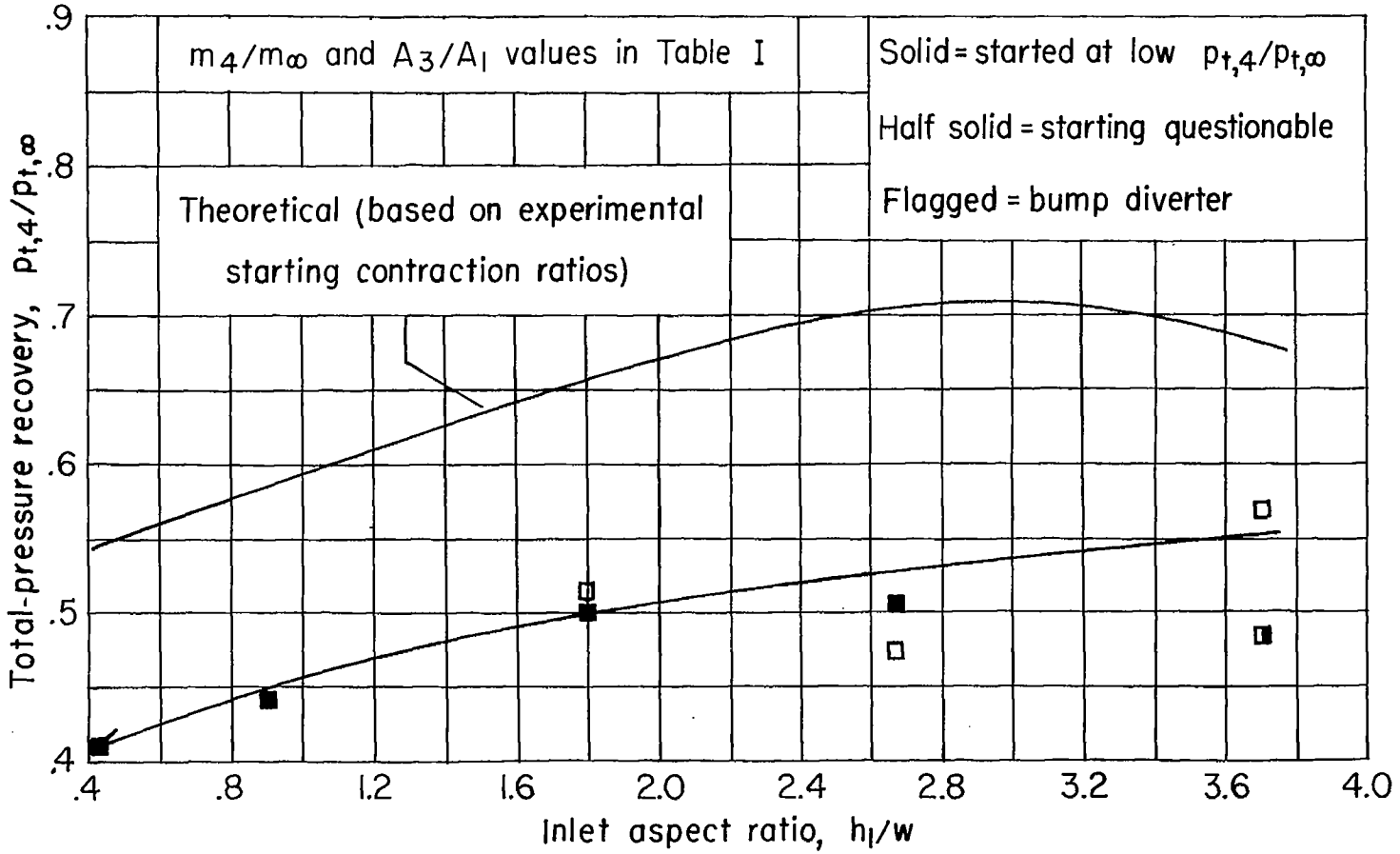

Figure 26.- Continued.

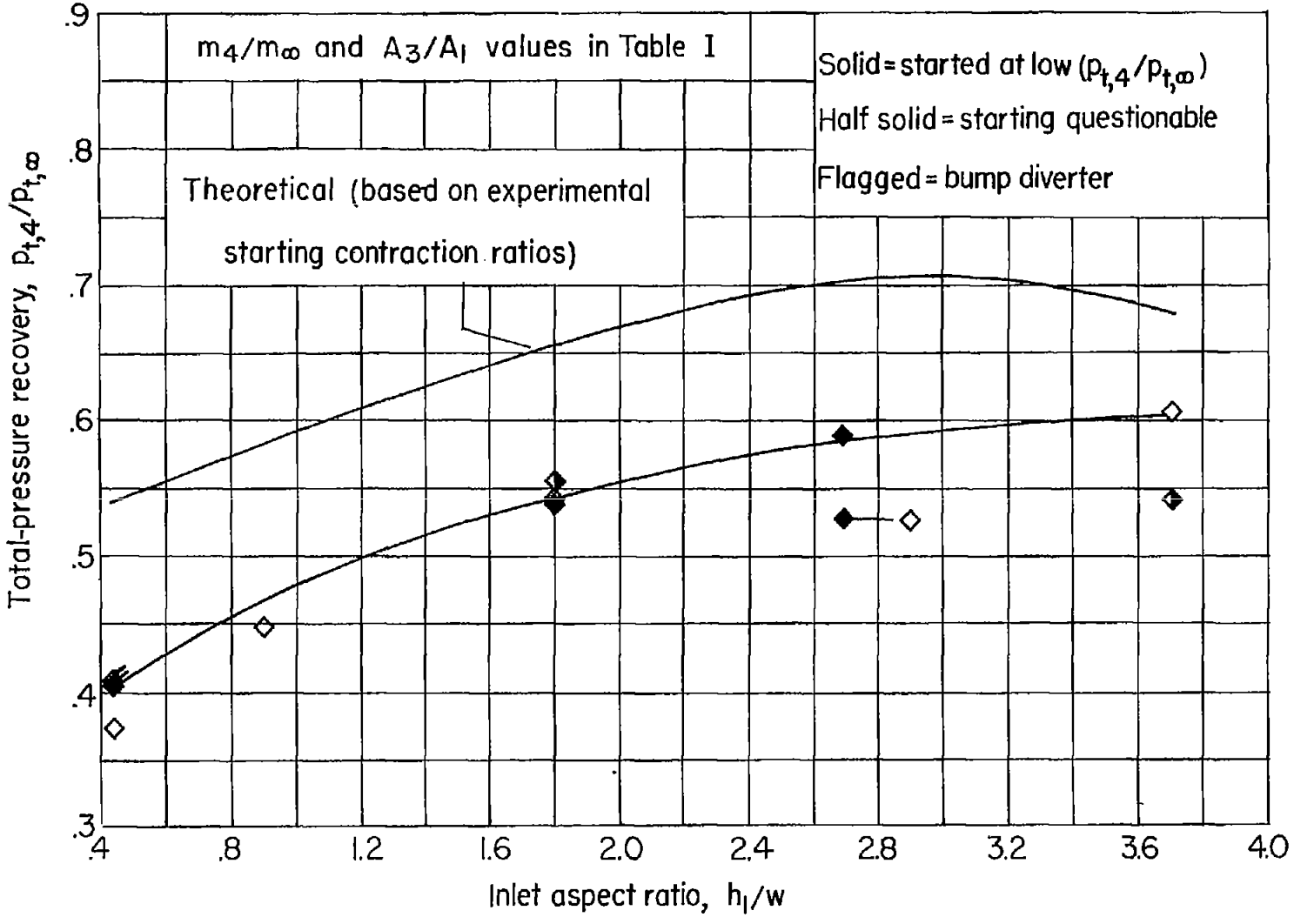

Figure 26.- Concluded.

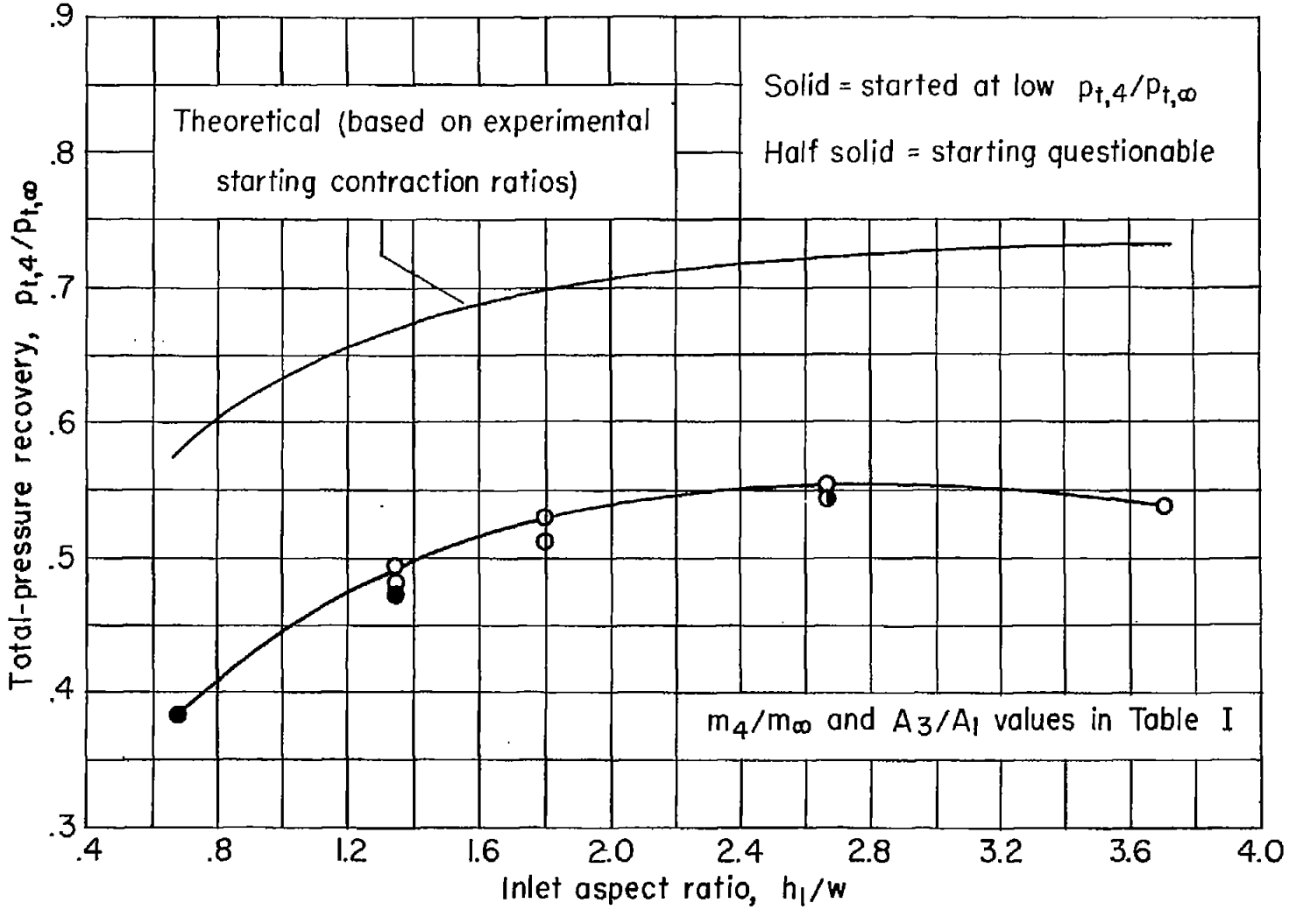

Figure 27.- Effect of inlet aspect ratio on the maximum total-pressure recovery with boundary-layer diversion. Diverter 2; $M_\infty = 3.1$.

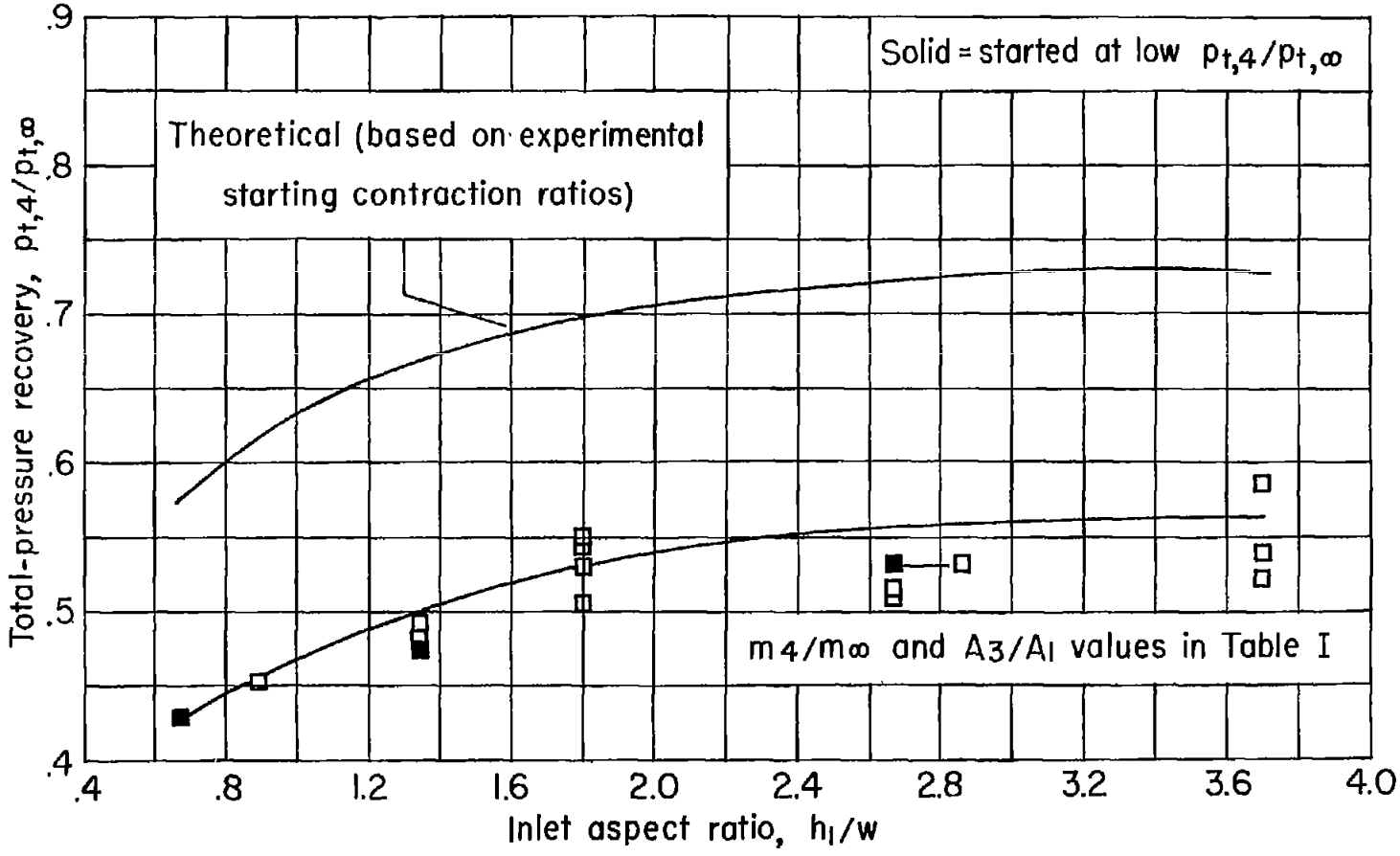

Figure 27.- Continued.

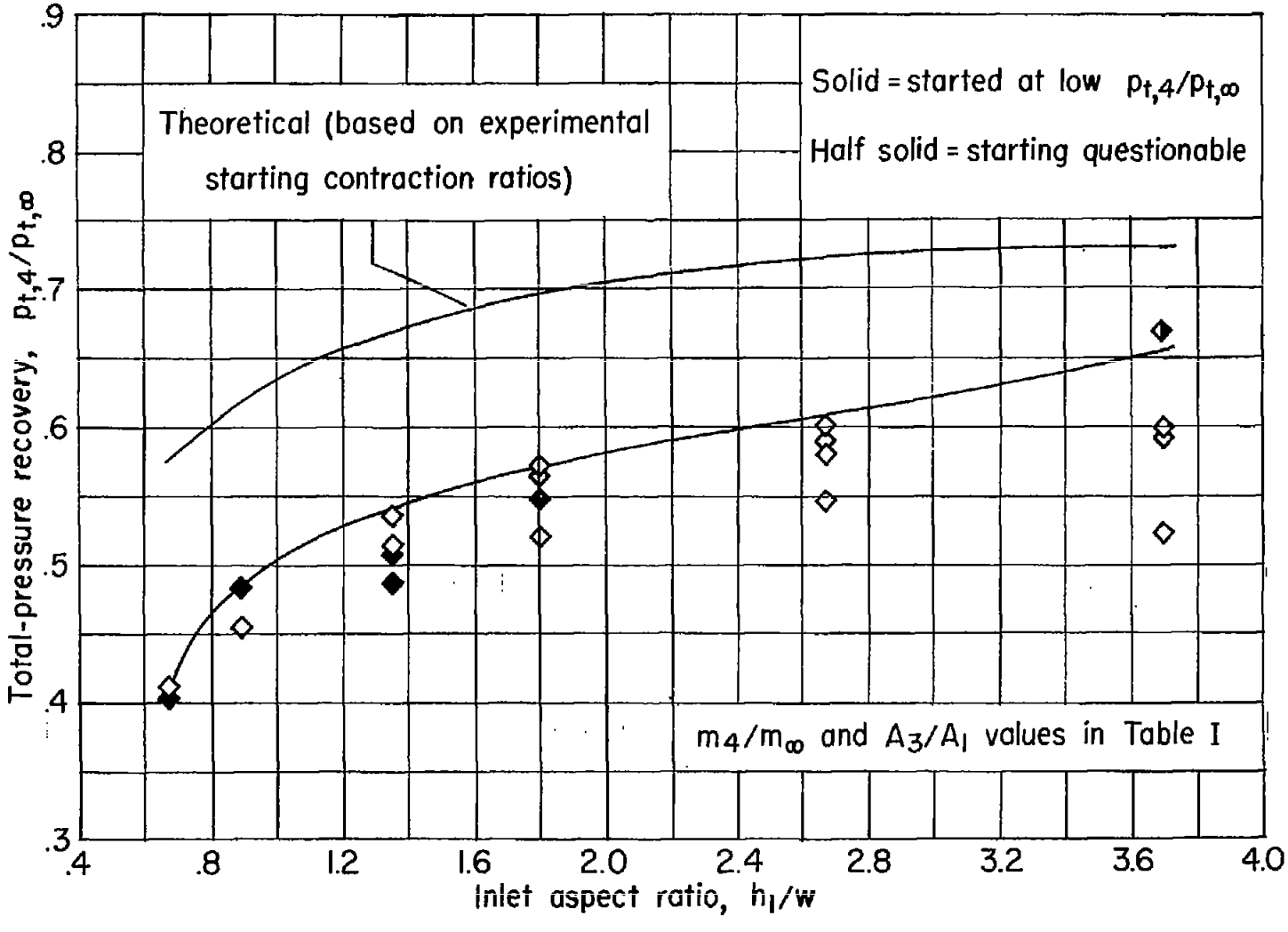

Figure 27.- Concluded.

NOTES: (1) Reynolds number is based on the diameter of a circle with the same area as that of the capture area of the inlet.

(2) The symbol * denotes the occurrence of buzz.

Report and facility	Description			Test parameters				Test data				Performance		Remarks
	Configuration	Number of oblique shocks	Type of boundary-layer control	Free-stream Mach number	Reynolds number $\times 10^{-6}$	Angle of attack, deg	Angle of yaw, deg	Drag	Inlet-flow profile	Discharge-flow profile	Flow picture	Maximum total-pressure recovery	Mass-flow ratio	
CONFID. RM L57J07 Langley Gas Dynamics Branch	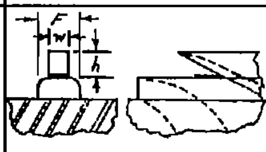	12° plus isentropic	None or flat-wedge diverter on fuselage	3.1	2.8 per inch or 3.0 to 9.1	0	0				✓	0.67 .55	0.65 .89 (overall range 1.0 to 0.13)	Swept scoop inlets of seven aspect ratios h/w, height h constant; three fuselage cross-sectional widths F tested. Minimum starting contraction determined.
CONFID. RM L57J07 Langley Gas Dynamics Branch	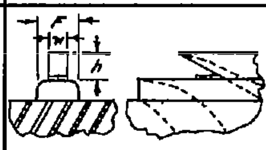	12° plus isentropic	None or flat-wedge diverter on fuselage	3.1	2.8 per inch or 3.0 to 9.1	0	0				✓	0.67 .55	0.65 .89 (overall range 1.0 to 0.13)	Swept scoop inlets of seven aspect ratios h/w, height h constant; three fuselage cross-sectional widths F tested. Minimum starting contraction determined.
CONFID. RM L57J07 Langley Gas Dynamics Branch	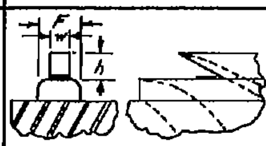	12° plus isentropic	None or flat-wedge diverter on fuselage	3.1	2.8 per inch or 3.0 to 9.1	0	0				✓	0.67 .55	0.65 .89 (overall range 1.0 to 0.13)	Swept scoop inlets of seven aspect ratios h/w, height h constant; three fuselage cross-sectional widths F tested. Minimum starting contraction determined.
CONFID. RM L57J07 Langley Gas Dynamics Branch	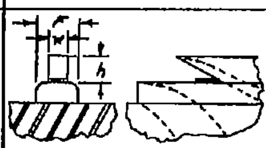	12° plus isentropic	None or flat-wedge diverter on fuselage	3.1	2.8 per inch or 3.0 to 9.1	0	0				✓	0.67 .55	0.65 .89 (overall range 1.0 to 0.13)	Swept scoop inlets of seven aspect ratios h/w, height h constant; three fuselage cross-sectional widths F tested. Minimum starting contraction determined.

Bibliography

These strips are provided for the convenience of the reader and can be removed from this report to compile a bibliography of NACA inlet reports. This page is being added only to inlet reports and is on a trial basis.